TWO-DIMENSIONAL CALCULATIONS

of

MAGNETIC MICROPULSATION RESONANCES

R J Greenfield

June 21, 1965

Project NR-371-401

Geophysics Laboratory
Massachusetts Institute of Technology
Cambridge 39, Massachusetts

TWO-DIMENSIONAL CALCULATIONS

of

MAGNETIC MICROPULSATION RESONANCES

R. J. Greenfield

June 21, 1965

Project NR-371-401

Geophysics Laboratory
Massachusetts Institute of Technology
Cambridge 39, Massachusetts

TWO-DIMENSIONAL CALCULATIONS OF MAGNETIC MICROPULSATION RESONANCES

by

ROY JAY GREENFIELD

S.B., Massachusetts Institute of Technology
(1958)

M.S., Massachusetts Institute of Technology
(1962)

SUBMITTED IN PARTIAL FULFILLMENT

OF THE REQUIREMENTS FOR THE

DEGREE OF DOCTOR OF

PHILOSOPHY

at the

MASSACHUSETTS INSTITUTE OF

TECHNOLOGY

June, 1965

Signature of Author.....Roy Jay Greenfield.....
Department of Geology and Geophysics, June 21, 1965

Certified by.....
Thesis Supervisor

Accepted by.....
Chairman, Departmental Committee on Graduate Students

TWO-DIMENSIONAL CALCULATIONS OF MAGNETIC MICROPULSATION RESONANCES

by

Roy Jay Greenfield

Submitted to the Department of Geology and Geophysics

on June 21, 1965 in

partial fulfillment of the requirements for the

degree of Doctor of Philosophy

ABSTRACT

Magnetic micropulsations in the period range of 5 to 45 seconds have been interpreted as a resonant amplification of waves in the ionosphere. The wave involved is of the type which is not guided by the earth's magnetic field. A resonance can occur, because the wave energy is trapped by the rapid increase with height of the Alfven wave velocity above the F_2 peak. Previous theoretical investigations of this resonance have been limited to models for the ionosphere in which the properties could only vary with height and not with horizontal position. This study considers the effect of horizontal variations, by examining the solutions of two-dimensional models.

Two such models are studied. The first simulates longitude independent propagation in a spherical earth-ionosphere. The horizontal variation is introduced by the inclusion of a dipole magnetic field. Solutions were studied separately for daytime and nighttime ionospheric conditions. Results show that the lowest frequency vertical mode of the one-dimensional model is replaced by a series of resonant modes in the two-dimensional model. Because of the dipole magnetic field, there are significant separations (up to 50 per cent) in the resonant frequencies of the lower order modes in the series. Studies based on one-dimensional, layered models predict frequencies which are higher than those observed at mid-latitudes; the use of two-dimensional models explains this discrepancy.

The second model is a cylindrical model. In this model the ionospheric parameters, such as the electron density, vary with the angular coordinate. Propagation is almost independent of the z coordinate and is representative of latitude independent propagation. Results obtained with this model show the continuous variation of the apparent period with local time, which is in agreement with observations of actual micropulsations. Results from this model show, in addition, that the energy from a subsolar source is confined to the daytime hemisphere.

Both two-dimensional models were solved by the use of finite difference methods. Relaxation techniques were found to be unsuitable for solving the set of linear difference equations, which arises in the numerical solution of a time-harmonic wave problem. A convenient direct method for solving such problems was developed.

The effect of the neutral atmospheric layer below the ionosphere was considered. The presence of this layer lowers the Q of the resonant peak and greatly decreases the surface magnetic field component perpendicular to the direction of propagation.

Thesis Supervisor: Theodore R. Madden

Title: Associate Professor of Geophysics

ACKNOWLEDGEMENTS

I wish to express my sincere thanks for the help and advice given to me by Professor T. R. Madden. Much of the direction taken by this thesis came about as a result of discussions with him and many techniques used in this investigation were learned in courses taught by Professor Madden.

My thanks also go to Professor A. F. Gangi for suggestions on the preparation of the manuscript and to Dr. T. Cantwell for his assistance during the course of this dissertation.

I give thanks to my wife, [redacted] for her help and encouragement while this dissertation was being written.

The manuscript was typed by Jeanette Braunhardt. Mrs. Joyce Medverd and Miss A. Dudley Templeton drew several of the figures and Joseph T. Procito, Jr., assisted in the preparation of several computer programs. All numerical computations were done on the IBM 7094 at the M.I.T. Computation Center.

I wish to acknowledge the financial support for this work which was given by the Office of Naval Research, Contract NR-371-401. The author held an American Chemical Society fellowship during the academic year 1963-1964 and previous to that a research assistantship sponsored by the Advanced Research Project Agency, contract AF 19(604)7378.

TABLE OF CONTENTS

TABLE OF CONTENTS (continued)

TABLE OF CONTENTS (continued)

TABLE OF CONTENTS (continued)

LIST OF FIGURES

LIST OF TABLES

CHAPTER I

INTRODUCTORY MATERIAL

1.1 Introduction

Over the last decade many authors have made contributions to the literature concerned with the measurements, characteristics and causal mechanisms of the rapid variations in the earth's electromagnetic field. Their interest stems from the light that the rapid variations may shed on processes in the ionosphere and from the use of natural signals as a tool for the exploration of the solid earth.

Rapid variations in the earth's electromagnetic field are known as magnetic micropulsations. These are small amplitude fluctuations characterized by periods of .2 sec to 10 min. This study will be concerned with quasi-sinusoidal micropulsations which sometimes show a well defined spectral peak and which have periods of 5 sec to 45 sec; these will be denoted by Pc 2,3.

The present state of knowledge of Pc 2,3 behavior will be discussed at length in the next section; here we list the known features which should be explained by a mathematical model of the Pc 2,3 mechanism.

1) The activity level is higher during the day than at night
2) The dominant period is highly dependent on local time and changes gradually
3) The daytime period is close to 20 sec, independent of latitude
4) Daytime Pc 2,3 extend over thousands of km
5) Nighttime periods are 5 sec to 10 sec.

Pc 2,3 oscillations are presumed by many authors to be characteristic of a resonant amplification of modified magnetohydrodynamic waves in the spherical shell cavity bounded below by the earth's surface and above by

a steep increase of the Alfven velocity between 400 km and 3000 km altitude. This cavity extends around the earth and may be thought of as lying between two concentric spherical shells. A cavity of this shape helps to explain why people observe Pc 2,3 disturbances over large areas. The magnetohydrodynamic wave which is involved in the resonance is the type which propagates isotropically (the fast type) and not the type which is guided by the magnetic field lines.

In this thesis mathematical models will be used to examine the manner in which the cavity responds to an excitation. There are several reasons to seek a thorough understanding of the cavity response. The first reason is to aid in the determination of the mechanism or mechanisms which excite micropulsations. A second incentive for investigating the cavity response is that the wave propagation characteristics are controlled by the state of the ionosphere; consequently the manner in which the signal changes with time can add to our knowledge of the ionosphere. In particular, we may obtain limits on the manner in which the electron density and the ion-neutral collision frequency vary with position. A final reason for the theoretical study of the cavity response is to acquire information which will enable us to determine which measurements would be useful in gaining further knowledge of the source and/or cavity. These measurements might be made on the surface, or, perhaps, certain satellite based measurements in the ionosphere might be important.

The previous mathematical models used to study the fast wave type were one-dimensional, plane, layered models. These models do not allow the media to vary in the horizontal direction. Results with these models predict a fundamental vertical resonant mode with a series of vertical

overtones. The period of the fundamental mode predicted by a model for daytime equatorial conditions is in agreement with the observed periods; however, the layered model predictions for mid and high latitudes give periods which are shorter than those observed. The layered models show that the difference between the daytime and the nighttime period is a result of the diurnal variation of ion-density.

The purpose of this thesis is to show that when the mathematical model conforms more closely to reality by allowing horizontal variations, the model can predict several features of the observations which are not predicted by layered models. The two models which are studied allow the media to vary in one horizontal direction as well as the vertical direction.

The first model of the earth-ionosphere system is a spherical model with no longitude dependence, and the earth's magnetic field is represented by a dipole. Therefore the wave propagation constant varies with latitude, as well as with height. Daytime and nighttime ionospheric conditions are studied separately and give similar conclusions about the mode structure. Each of the modes of the layered models becomes a sequence of modes in the two-dimensional models. This study concentrates on the series of horizontal modes which replace the fundamental modes of the layered models. Due to the dipole field, the resonant frequency increases for successive horizontal modes. For both day and night conditions the frequency of the fifth horizontal mode is 47 per cent higher than the frequency of the first.

The period of the first mode is determined by the values of the propagation constant at the equator and this period is in agreement with the observed daytime period. A low latitude source will excite the first mode to a much greater degree than it will excite other modes. An interpretation

of daytime Pc 2,3 as an oscillation of the first mode will explain the observed period and the independence of period with latitude.

The second model studied was a cylindrical model for the earth-ionosphere system. The ionospheric parameters are continuous functions of the angular coordinate and, as such, represent the change from daytime to nighttime and vice versa. The propagation in this model is almost independent of the z coordinate which is taken along the earth's magnetic dipole axis; therefore, this type of propagation is a model for latitude independent propagation.

In the daytime and nighttime portions of the real cavity the observed periods are different. Results with this second model show the observed diurnal variation of period. The model results show a gradual change of period with local time; this is in agreement with observations. When this model was excited with sources in the daytime hemisphere the response was confined to that hemisphere. If the real sources are more active in the daytime side of the ionosphere, this model predicts, in agreement with the observed diurnal level of activity, that the daytime level of micropulsation activity will be higher than the nighttime level.

Computational considerations imposed certain limitations on the models. The models did not include the Hall conductivity, and the model geometries were such that only the isotropic wave type, and not the guided wave type, was excited. The effects of these limitations are considered. The magnetic field of the waves in the models has no eastward component. Therefore, no useful information can be obtained about the surface field polarization.

1.2 Review of Observations

Main Observational Features of Pc 2,3

The characteristics of Pc 2,3 micropulsations, which in this author's opinion have been established, are:

1) daytime periods of Pc 2,3 are generally between 16 sec and 24 sec
2) the daytime period is independent of latitude
3) daytime Pc 2,3 disturbances extend for thousands of km
4) the periods at night are 5 sec to 10 sec
5) the transition from daytime to nighttime periods is gradual
6) The level of activity is higher during the day than at night

Three Pc 2,3 characteristics, which reflect the cavity properties but which have not been systematically reported, are:

1) the values of the Q's of the Pc 2,3 spectral peaks
2) the variation of amplitude with position
3) the relative phase of the oscillations at different stations.

The published observational data supporting these conclusions are given below.

Micropulsation Notation

The Pc 2,3 is only one of a number of types of magnetic micropulsations. In this section we describe the method of classifying micropulsations which is presently in use (see Jacobs et al. [1964]). Micropulsations are divided into two major divisions: Pc and Pi.

The Pc are quasi-sinusoidal oscillations which repeat for many cycles without great change in either amplitude or period. Pc are further divided by period as shown in Table 1.2-1:

TABLE 1.2-1

Notation for Division of Pc into Frequency Ranges

	Period Range
Pc 1	.2 to 5 sec
Pc 2	5 to 10
Pc 3	10 to 45
Pc 4	45 to 150
Pc 5	150 to 600

Because Pc 2 and Pc 3 are believed to be the nighttime and daytime manifestations of the same phenomena, the notation Pc 2,3 is being used in this thesis to denote the whole range of periods covered by Pc 2 and Pc 3. Saito (1964) introduced this notation.

The Pi notation is used for signals that are transient and irregular in nature. The Pi have been divided into two period ranges: Pi 1 having periods of 1-40 sec and Pi 2 having periods of 40-150 sec.

Daytime Period

The earliest systematic study of the Pc 3 micropulsation was that of Holmberg (1951). He designated the period of the signal as the average time between maxima. Using data from approximately one hundred disturbances, he formed histograms of occurrence frequency versus period. The results showed that most daytime Pc 3 signals had periods between 17 and 26 sec.

Using records from widely separated areas of the earth, several other authors since Holmberg have analyzed records in a similar manner. Maple (1959) used records from Tucson, Arizona, and found Pc 3 activity having periods from 15 to 25 sec. Bolshakova and Zubin (1961) used data from three Russian stations and found 20 sec to be the most commonly observed period for Pc 3. Oshima (1960) found this also to be true in Japan, while Campbell (1959) found 22 sec to be the most commonly observed period for Pc 3 in California. Data given by Saito (1964) showed that 85 per cent of the Pc 3 oscillations observed at Fredericksburg, Virginia, had periods between 18 and 23 sec. The most common period was 20 sec. All the Pc 3 observed occurred during the daylight hours. From a review of several authors' work Saito concluded that the daytime period was nearly independent of time of year, phase of the solar cycle, and latitude.

Duncan, (1961) using a sonograph to analyze records, found the most likely noontime periods to be 23 sec at Adelaide and 19 seconds at Townsville, Australia. At Adelaide, 85 per cent of the periods lay

between 18 and 28 sec. At Townsville, 70 per cent of the periods lay between 17 and 26 sec.

The number of period determinations made from visual inspection of chart records is much greater than the number of power spectra which have been computed. The available power spectra do, however, show periods generally consistent with the visual determinations.

Smith et al. (1961) show a spectral peak having an 18 sec period for both the electric and magnetic field records taken at Austin, Texas. Bostick and Smith (1962) find a spectral peak at 25 sec period, also using Austin records. Davison (1964) computed power spectra for 55 daytime records from New Jersey and reports a daytime spectral peak at approximately 26 sec periods; no information on the variability of the period was given.

In October, 1962, a series of nine simultaneous daytime and post-midnight electric field measurements was taken at Trinidad, Austin, and Puerto Rico; spectral analyses and coherencies were computed for the measurements. The results of the analyses are reported by Orange and Bostick (1964), and also by Prince, Bostick, and Smith (1964). The majority of the spectra had peaks between 20 sec to 35 sec. Coherency computations between stations were available for three of the records and showed high coherencies near the frequencies of these peaks. Several of the spectra also showed a second peak at much lower power levels for periods of less than 14 sec. For each recording interval, Prince, Bostick, and Smith (1964) give a quantity they denote as "the

apparent dominant period" of the Pc 2,3. Evidently, this quantity is a visual determination of the period from the chart records. These periods correlated very well with the periods of the spectral peaks. The frequency analyses of the records from each station taken on October 13, 1962, from 1030-1115 UT showed a spectral peak at .045 cps (22 sec period). The coherency between the Austin (42°N latitude) and Trinidad (20°N latitude) records was .95 at frequencies near the spectral peak. Trinidad is a low magnetic latitude station; therefore this work supports Saito's statement that the Pc 3 period is independent of latitude.

It has been observed by Saito (1960), Maple (1959), and Duncan (1961), that the period of the daytime Pc 3 oscillations decreases during magnetic storms. It is known (see Ratcliffe [1960]) that the ion density in the F_2 region often decreases during storms. This decrease of ionization may be the cause of any decrease of periods which occurs during storms.

Q of Spectral Peaks

Not enough power spectra are available to make any definite statement about the Q of the Pc 3 spectral peak. The few available spectra give values as follows.

The highest values of the Q for the Pc 3 peaks found by Orange and Bostick (1965) were approximately 2; some of the peaks were of much lower Q. Bostick and Smith (1962) found a Pc 3 peak with a Q of 2. Smith et al. (1961) found a peak with a Q of 4. No nighttime

spectra are available.

Extent of Disturbances

There is good evidence that daytime Pc 2,3 micropulsations extend for large distances. Jacobs and Sinno (1960) found simultaneous activity at stations in the western hemisphere from the Arctic to the Antarctic. Madden (1965) recorded activity at Cambridge, Massachusetts, that was almost identical to the activity at La Jolla, California. Santirocco and Parker (1963) described Pc 2,3 measured in Bermuda as virtually identical with those measured in Rochester, New York. Kato and Watanabe (1957) observed similarities in signals recorded in France and in Madagascar. Prince, Bostick, and Smith (1964) report frequent similarity between Pc activity at Austin, Texas and La Grande, Oregon. Orange and Bostick (1965) found high coherencies at Pc 2,3 frequencies among the signals recorded at Austin, Puerto Rico, and Trinidad.

Amplitude Dependence on Latitude

There has been some discussion of amplitude dependence on latitude using simultaneous Pc 3 measurements. Jacobs and Sinno (1960) report simultaneous Pc activity at several stations from Sitka to Little America on May 7, 1958. The maximum amplitude was judged to be near latitudes of 40°. Ellis (1961) used three Australian stations between 30° and 50° latitude and found Pc 3 amplitude increased moderately with latitude.

The evidence for daytime Pc 2,3 amplitude dependence on latitude appears to be uncertain at present. Additional, controlled observations will be necessary before any definitive statement can be made. No studies have been made on nighttime amplitudes.

Nighttime Behavior

The nighttime behavior of micropulsations is considerably different from that of the daytime behavior. The level of activity is much lower and continuous pulsations are not common. Some observations of nighttime Pc 2,3 have, however, been reported. Yanagihara (1960) observed Pc 2 (termed SPC in his work) having periods of 8 to 10 sec. Maple (1959) notes Pc 2 type activity in the nighttime having periods around 8 sec. Campbell (1959) gives 5 sec as the period of nighttime micropulsations. Kato and Saito (1959) found the Pc 2,3 periods were 6 sec to 10 sec at night.

The resonant properties of the cavity may be inferred from Pi 1 activity, as well as from Pc 2 nighttime activity. Yanagihara (1960) observed that oscillations of Pi 1 (termed SPT by Yanagihara) having periods of 6 to 10 sec accompanied Pi 2. The Pi 1 periods were shown to be independent of the period of Pi 2. Troitskaya (1964) described a nighttime phenomenon, which she termed SIP, which appears to be the same phenomenon as Yanagihara's SPT. This same type of disturbance is designated as type B by Benioff (1960); he found it associated with K_p index and auroral intensity.

Day to Night Transition

The transition of Pc 2,3 oscillations from the daytime Pc 3 periods to nighttime Pc 2 periods was studied by Kato and Saito (1954). Figure 2.1-1 shows their plot of the diurnal variation of the Pc 2,3 period. These authors also give a plot of the rapid pulsation accompanying 26 sudden storm commencements and 5 sudden impulses, and a plot of the shortest period pulsations occurring during 4 magnetic storms. The 3 plots show similar diurnal behavior; the longest periods occur near noon. For the first two phenomena the longest periods averaged 18 sec, while the nighttime periods were 7 to 10 sec. From 10 hrs to 16 hrs local time more than 90 per cent of the oscillations had periods between 16 and 21 sec. The periods during the storms averaged one or two seconds shorter. The changes from nighttime to daytime periods and vice versa occurred gradually over a period of several hours.

This continuous change of period from day to night has been studied with the use of sonographs to monitor the oscillation periods for several hours. A record taken and analyzed by Duncan (1961) showed continuous activity on the 7th of September, 1960, lasting from 06 hrs local time to 18 hrs local time. The period was 14 sec at 06 hrs, rose to 20 sec at noon, then remained constant until 18 hrs. Saito (1960) gives a sonagraph analysis for 12 hrs local time, June 3, 1957, in which the maximum power in the signal is at 20 sec period. In a sonagraph analysis made at 19 hrs that day, the power was centered around 15 sec periods. These results support the evidence for continuous period change found by Kato and Saito.

Figure 1.2-1

Diurnal Variation of Pc 2,3 Period

Taken from Kato and Saito (1959)

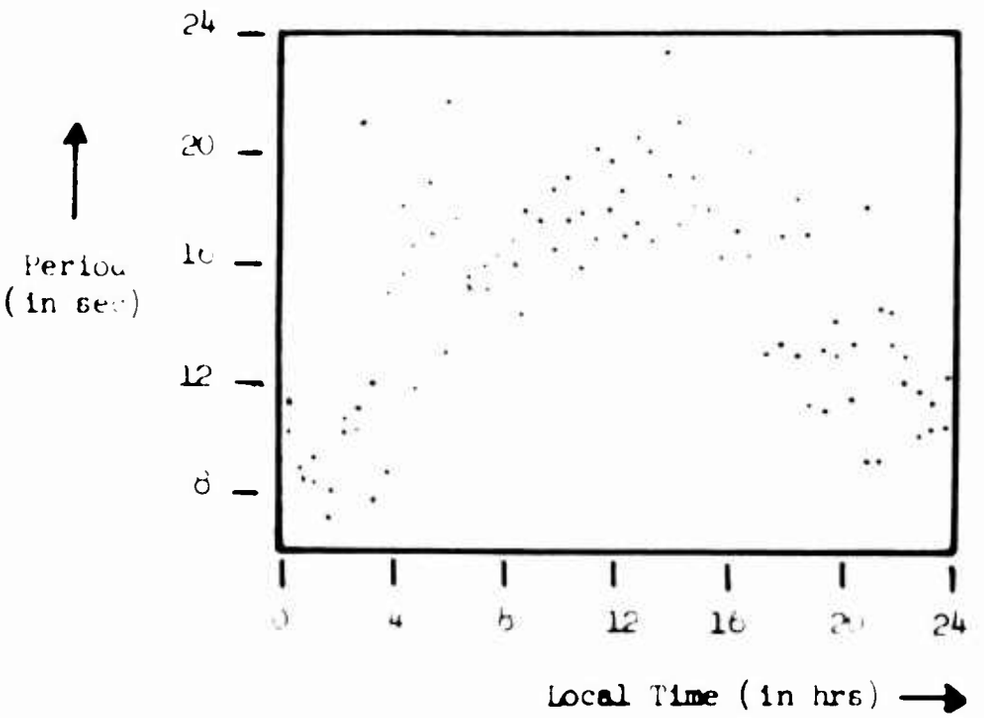

Ness et al. (1962) made a study of the diurnal variation of the period of micropulsations in the Pc 2 and Pc 3 frequency ranges. The dependence of period on local time which is shown in their results is different from that found by other investigators.

Diurnal Variation of Occurrence Frequency and Activity

Pc 3 are a very common feature of daytime records. Holmberg (1951) found that both the occurrence frequency and average amplitude of Pc 2,3 was higher during the day than at night. Saito's (1964) data shows that the Onagawa observatory observes Pc 2,3 more than 60 per cent of the observing time during the summer months at hours around noon. Yanagihara's (1960) data shows that 90 per cent of the Pc 3 recorded at Memambetsu occur between 6 hrs and 18 hrs local time. At both Onagawa and Memambetsu, Pc 2,3 is seen less than 10 per cent of recording time during the hours around midnight.

Several authors have given rather involved quantitative definitions for the quantity activity. The meaning of activity as they define it is roughly the integral of the signal amplitude divided by the total recording. Yanagihara (1960) shows that the highest activity levels occur from 9 hrs to 12 hrs local time and that the highest daytime level is 5 or 6 times the nighttime level. Saito (1964) shows negligible activity at Fredericksburg, Virginia, during the nighttime.

1.3 Previous Theories of Pc Type Magnetic Micropulsations

This section gives a brief review of the previous attempts to explain micropulsations. All of the theories assume that micropulsations

are the consequence of resonant trapping of magnetohydrodynamic wave energy in the ionosphere (many authors use the term exosphere for the outer portion of the ionosphere where hydrogen ions predominate).

Holmberg (1951) considered several possibilities for systems which might resonate at periods near 20 sec. He studied several electromagnetic systems in the unionized air layer below the ionosphere, and concluded the resonant periods of these systems would be too short. He also considered vertically traveling magnetohydrodynamic waves, which might be trapped in one of the ionospheric layers. In this analysis the value for the Alfven velocity was calculated using the neutral atmospheric density, rather than the ion mass density. This procedure led to periods many times greater than 20 seconds.

Dungey (1954) showed that in the outer ionosphere, where particle collisions could be neglected, the behavior of magnetohydrodynamic waves can be determined by solving a pair of coupled partial differential equations. It was shown that if the solutions were symmetric about the magnetic polar axis, i.e., longitude independent, the equations were uncoupled. One equation governs the propagation of a mode having only an eastward component of the electric field. This mode is often referred to as the poloidal mode. Dungey used travel time arguments to suggest that poloidal resonances of the whole exosphere would have a fundamental period of an hour. Kato and Watanabe (1958) came to similar conclusions about the poloidal mode period. The second equation governed the propagation of a mode having only an eastward component of the perturbing magnetic field and of the particle motion. This mode, called

the toroidal mode, is guided by the magnetic field lines. Estimates were made of the periods of the toroidal mode as a function of latitude. Dunge 's toroidal modes are still used to explain high latitude oscillations with several minute periods. Westphal (1961) has made further computations of the toroidal mode periods.

Maple (1959) suggested that hydrodynamic waves trapped in the E or F layer might cause the Pc oscillations, but he failed to give an quantitative argument about the periods.

Dessler (1958) pointed out that hydromagnetic waves would have a large phase velocity at a few thousand km height. The velocity increases because the charged particle mass density decreases from its value in the F_2 region due both to the decrease in number density and the transition from Oxygen to Hydrogen as the predominant ion. At greater heights the decrease in the dipole magnetic field becomes important and the velocity again decreases. Several authors, apparently beginning with Yanagihara (1960), have considered, qualitatively, the resonances which might be caused by energy trapped below the high phase velocity region.

MacDonald (1961) calculated the longest resonant period of magnetically guided collisionless waves as twice the travel time along a line of force. Two cases were considered. In the first case, energy trapped on the whole length of a line of force of the earth's dipole field was considered. The resonant periods found were highly latitude dependent. The periods of the fundamental mode varied from 14.2 sec at 3^{0} latitude

to 184.6 sec at 60° latitude. In the second case, energy trapped between the F_2 region and the high Alfven velocity region was considered. In this case the periods varied from 10.8 seconds at 35° latitude to 6.7 sec at 60° latitude. Jacobs and Watanabe (1962) used matrix methods to find the resonant amplifications, caused by trapping below the high velocity region, of incoming plane waves. The calculations were made for guided Alfven waves traveling parallel to a vertical magnetic field. The magnetic field value was the polar region value. The longest period found, that for the low Alfven velocity model, was 8.5 seconds.

A group at the University of Texas performed a series of theoretical investigations into the resonant amplification of plane waves impinging from the outer exosphere. Their model studied the fast (extraordinary mode) wave type. Little coupling with the guided type (ordinary mode) was noted. In these papers the magnetic field and ionospheric parameter were independent of horizontal position, allowing plane wave solutions. The ionospheric models were represented by homogeneous layers and matrix methods were used to obtain the response on the ground. In the first of these papers, Prince and Bostick (1964) studied several ionospheric models with vertically propagating waves for an equatorial magnetic field. Their results showed that the longest resonance period for a reasonable daytime model would be near 20 seconds.

Prince, Bostick, and Smith (1964) showed that a wave propagating with a moderate north-south wave number through an equatorial magnetic field model had the same resonant frequency as had been found for vertical

propagation. When the magnetic field represented the stronger field at middle latitudes, however, the resonant frequency increased to about .085 cps. (period = 12 sec).

To investigate the height at which reflection of energy occurs at the top of the cavity, Prince, Bostick, and Smith (1964) carried out computations with the model terminated at 1000 km height. The termination was a uniform half space; no energy could, of course, be reflected above 1000 km in this model. Results obtained from the use of this model showed the same resonant frequencies as results obtained from models in which the layering extended to 2000 km. This indicated that the effective top is below 1000 km, and the energy reflection is probably associated with the rapid decrease of ion mass associated with the transition from Oxygen to Hydrogen ions.

Li, Prince, and Bostick (1964) considered nonvertical propagation in the north-south vertical plane for magnetic fields corresponding to 38° and 90° magnetic latitudes. Several angles of incidence were considered. The results demonstrated that the angle of incidence is not important and that the magnetic field strength determines the resonant frequency for a given ionospheric model.

1.4 Method of Investigation and Thesis Outline

Method of Investigation

The response of the cavity to harmonic sources is to be examined. Ideally, to carry this out we would obtain an analytic solution to the equations which govern electromagnetic propagation in the cavity. The cavity is, however, a three-dimensional region in which the properties change greatly. Because of these complications, the possibility of an analytic solution seems remote. Use of a layered model, such as the one used by Thompson (1963), would not allow horizontal variation of the propagation properties and so would not greatly add to the plane wave results. The well known WKB method is not applicable, because of the great changes of the media over a wave length.

The solution can, however, be approached by approximating the relevant partial differential equations by finite difference equations. The finite difference equations are a set of linear equations whose solution gives an approximation to the solution of the original problem. The use of finite difference equations is very closely related to the impedance concept used by Madden and Thompson (1964).

To gain suitable accuracy in the three-dimensional region, the number of linear equations must be on the order of thousands. The amount of computation required to obtain a solution would, therefore, be very large. To avoid the extremely lengthy computations involved in solving a three-

dimensional model, the horizontal variations which occur with latitude and longitude were studied separately through the use of a pair of two-dimensional models. The two models which were studied have the common computational advantage that the fast and guided modes are uncoupled and, therefore, the solution of the models requires the solution of a scalar, and not a vector, two-dimensional partial differential equation.

Description of Chapter II

Before describing the two models which are studied in chapters III and IV, we will describe the contents of chapter II. This chapter deals with topics related to the properties of Pc 2,3 frequency waves in the ionosphere, including the question of coupling between the wave types.

In the first section we present the models for the ionospheric parameters which are used in the chapters III and IV computations. In the next section the propagation characteristics of Pc 2,3 frequency plane waves, at different altitudes in the ionosphere, are reviewed.

Because of the geometry of the models in chapters III and IV, no coupling occurs between the fast and guided wave types. In the third section of chapter II the importance of coupling in the more general case is considered.

Finally, in the last section we discuss the effect of the Hall conductivity and consider what error is introduced because the Hall conductivity is not included in the chapter III and IV models.

Description of Chapter III Model

The model in chapter III is used to study the effect of the variation, with latitude, of the wave propagation constant. This latitude variation reflects the fact that the earth's magnetic field strength varies with latitude. The investigation is carried out with a spherical model with no latitude dependence. Solutions for daytime and nighttime ionospheric conditions are examined separately.

Description of Chapter IV Model

The model studied in chapter IV is a cylindrical model. In this model the ionospheric parameters show continuous variation from daytime to nighttime conditions. This model was chosen to examine the existence of different daytime and nighttime resonant frequencies in a single cavity and to show that a daytime source will not excite Pc 2,3 in the nighttime hemisphere.

In appendix I it is shown that the component of the surface magnetic field, perpendicular to the direction of propagation, is almost completely destroyed by the unionized air layer below the ionosphere. Because of this, a small modification was made to the chapter IV model.

Numerical Solution of Models

The description of the finite difference grids which were used to solve the models of chapters III and IV are given in appendixes II and III, respectively. Several aspects of the numerical work involved in solving the difference equations were applicable to both models. Each

of these aspects was made in a separate appendix:

In appendix IV we give the algorithm developed to solve the set of linear equations which arises from the finite difference method.

In appendix V we show that these linear equations cannot be solved with a relaxation method.

In appendix VI we analyze the error due to the grid spacing used in the finite difference method.

CHAPTER II

CHARACTERISTICS OF ELECTROMAGNETIC WAVES AT Pc 2,3 FREQUENCIES

2.1 Models for Ionospheric Parameters

Purpose of Ionospheric Models

In this section we will present the models for the ionospheric parameters which will be used in the computations of chapters III and IV. The models are given at this point so that the parameter values will be available in the next section in which ionospheric wave propagation will be discussed.

The majority of the computations will be carried out using the parameter values of a basic daytime model and a basic nighttime model. Since the major emphasis in this thesis is on the investigation of the effect of horizontal variations rather than the study of Pc 2,3 under widely varying ionospheric conditions, the values in the basic models have been selected to represent intermediate daytime and nighttime conditions. These models will be discussed below. Three modified versions of the basic daytime model will also be discussed below.

Basic Daytime Model

In Table 2.1-1 the values of the ionospheric parameters for the basic daytime model are given. This model will at times be referred to simply as the daytime model.

The daytime model values of N_e for the F region approximately follow values given by Sagalyn et al. (1963). Below the F region the values are similar to a profile given by Friedman (1964). The quantity $N_m F_2$, the maximum value of N_e in the ionosphere, is a meaningful quantity to use in discussing the variation of the electron density profiles. The value of $N_m F_2$ in the daytime model is 2.1×10^6 electrons/cc. Other daytime profiles show that the range of $N_m F_2$ is from $1. \times 10^6$ electrons/cc (see

TABLE 2.1-1

Daytime Model for Ionospheric Parameters and Modifications

	Basic Daytime Model						MCFL Model	MEPDI Model
	Radius km	Height km	N_e cc^{-1}	Average Molecular Weight	γ_e sec^{-1}	γ_i sec^{-1}	γ_i sec^{-1}	$N_e \times 10^{-6}$ cc^{-1}
1	6380.0	0.	.0000E 00	0.	.000E 00	.000E 00		
2	6480.0	100.0	.8000E 05	27.5	.600E 05	.100E 04	3000.	.04
3	6510.0	130.0	.1200E 06	26.5	.400E 04	.600E 02	60.	.06
4	6540.0	160.0	.1500E 06	23.0	.150E 04	.120E 02	12.	.075
5	6580.0	200.0	.3500E 06	20.5	.800E 03	.250E 01	4.	.175
6	6620.0	240.0	.8000E 06	19.0	.500E 03	.800E 00	2.	.32
7	6660.0	280.0	.1500E 07	18.0	.600E 03	.350E 00	.7	1.20
8	6700.0	320.0	.2100E 07	17.0	.800E 03	.160E 00	.3	
9	6750.0	370.0	.1750E 07	16.8	.800E 03	.600E-01	.11	
10	6830.0	450.0	.1100E 07	16.5	.500E 03	.250E-01	.025	
11	6960.0	580.0	.4000E 06	16.0	.200E 03	.000E 00		
12	7080.0	700.0	.1500E 06	15.0	.100E 03	.000E 00		
13	7230.0	850.0	.5600E 05	13.5	.700E 02	.000E 00		
14	7380.0	1000.0	.3500E 05	9.0	.500E 02	.000E 00		
15	7580.0	1200.0	.2350E 05	2.2	.200E 02	.000E 00		
16	7880.0	1500.0	.1500E 05	1.5	.100E 02	.000E 00		
17	8380.0	2000.0	.8200E 04	1.0	.700E 01	.000E 00		
18	9880.0	3500.0	.3000E 04	1.0	.500E 01	.000E 00		
19	11380.0	5000.0	.1900E 04	1.0	.300E 01	.000E 00		
20	12380.0	6000.0	.1500E 04	1.0	.200E 01	.000E 00		

Martyn [1959]) to 3. x 10^6 electrons/cc (see Nisbet and Bowhill [1960] and Millman et al. [1964]). This range indicates our profile is an intermediate electron density profile.

The ion-neutral collision frequencies, ν_i, which are given in Tables 2.1-1 and 2.1-2, were calculated from the expression

$$\nu_i = 2.6 \times 10^{-9} \quad N_n/M_i^{1/2} \qquad 2.1.1$$

Where N_n is the number of neutral particles per meter^3 and M_i is the ion molecular weight. Expression 2.1.1 was given by Chapman (1956).

The values of N_n used in calculating the daytime model values of ν_i were taken from Nicolet's (1961) model atmosphere number 7. Jachia (1962) found that model 7 gives the proper neutral density profile at the subsolar points when the level of solar radiation is low. For higher levels of solar radiation N_n will have greater values at altitudes above 200 km. Since ν_i is proportional to N_n, the daytime model values of ν_i are probably below average values for subsolar conditions.

The values of ν_i which follow from model 7 were used in the daytime model, because when computations were made using higher values the spectral peaks were relatively flat and the resonant frequency was hard to judge precisely. The effect of varying the values of ν_i was assessed by comparing spectra, computed for the modified models presented below with the daytime model spectra. When higher values of ν_i are used the resonant frequencies are not affected, but the Q's are lowered.

Nighttime Model

In Table 2.1-1 the values of the ionospheric parameters for the nighttime model are given. The nighttime profile of N_e is similar to the Johnson (1961) profile for sunspot maximum conditions. Johnson gives his profile as an example of an extremely high nighttime electron density profile. In this profile $N_m F_2$ has a value of $4. \times 10^5$ electrons/cc. Nisbet and Bowhill (1960), however, found values of 5.5×10^5 electrons/cc and $8. \times 10^5$ electrons/cc in measurements made near midnight during May, 1959. Therefore, Johnson's profile is not an extreme profile and a profile similar to his is a suitable intermediate value profile to use in the present investigation.

The values of ν_i for the nighttime model were calculated using expression 2.1.1. The values of N_n were taken from Nicolet's (1961) atmospheric model number 5. Jachia (1962) found that this model fits nighttime conditions at intermediate levels of solar radiation.

Modified Daytime Models

Three modified versions of the basic daytime model for the ionosphere were studied in chapter III.

The first modified model is used to assess the effect on the resonant frequency which results from a change in the values of ν_i. This model will be referred to as the MCFD (modified collision frequency daytime) model. The model is identical with the basic model with the exception that the values of ν_i in the MCFD model are higher between 200 km and 270 km. The modified values of ν_i in the model are given in the

TABLE 2.1-2

Nighttime Model for Ionospheric Parameters

	Radius km	Height km	N_e cc^{-1}	Average Molecular Weight	γ_e sec^{-1}	γ_i sec^{-1}
1	6380.0	0.	.0000E 00	0.	.000E 00	.000E 00
2	6480.0	100.0	.1200E 04	27.0	.460E 05	.300E 04
3	6510.0	130.0	.2200E 04	25.5	.300E 04	.140E 03
4	6540.0	160.0	.2500E 04	24.0	.400E 03	.230E 02
5	6580.0	200.0	.3000E 04	21.0	.200E 03	.560E 01
6	6620.0	240.0	.5300E 04	17.5	.100E 03	.220E 01
7	6660.0	280.0	.1600E 06	17.0	.200E 03	.920E 00
8	6700.0	320.0	.3400E 06	16.9	.300E 03	.440E 00
9	6750.0	370.0	.4000E 06	16.7	.300E 03	.170E 00
10	6830.0	450.0	.3400E 06	16.4	.200E 03	.400E-01
11	6960.0	580.0	.1800E 06	15.2	.150E 03	1.000E-02
12	7080.0	700.0	.7600E 05	13.5	.100E 03	.000E 00
13	7230.0	850.0	.3100E 05	9.5	.700E 02	.000E 00
14	7380.0	1000.0	.2100E 05	3.8	.500E 02	.000E 00
15	7580.0	1200.0	.1600E 05	1.9	.200E 02	.000E 00
16	7880.0	1500.0	.1000E 05	1.3	.100E 02	.000E 00
17	8380.0	2000.0	.6200E 04	1.0	.700E 01	.000E 00
18	9880.0	3500.0	.2700E 04	1.0	.500E 01	.000E 00
19	11380.0	5000.0	.1700E 04	1.0	.300E 01	.000E 00
20	12380.0	6000.0	.1400E 04	1.0	.200E 01	.000E 00

next to the last column of Table 2.1-1.

In the second modified model the only change from the daytime model is that the electron number density is lower below 280 km. The values of N_e below 280 km in this model are given in the last column of Table 2.1-1. This model will be referred to as the MEPD1 (modified electron profile daytime 1) model and is used to show the effect of lower values of conductivity in the lower ionosphere.

The third modified model was used to investigate the effect of a localized perturbation of the electron density upon the resonant frequency. The model is identical to the basic daytime model with the exception that the electron density varies with latitude at altitudes between 240 km and 1000 km. The values of N_e at the co-latitudes 70°, 64°, and 57° are given in Table 2.1-3. At co-latitudes outside this range the values of N_e in this model have the same values as in the basic daytime model.

TABLE 2.1-3

Modified Values of N_e for MEDP2 Model

N_e in units of 10^6 electrons/cc

θ = co-latitude

Height in km	N_e Basic Model	N_e $\theta = 70^\circ$	N_e $\theta = 64^\circ$	N_e $\theta = 57^\circ$
240	.8	.844	.865	.850
280	1.5	1.59	1.68	1.64
320	2.1	2.31	2.52	2.42
370	1.75	2.05	2.32	2.18
450	1.1	1.32	1.54	1.43
580	.4	.463	.495	.479
700	.056	.0605	.0650	.0628
1000	.035	.0364	.0378	.0372

2.2 Review of Ionospheric Wave Propagation

In this section we will review briefly the propagation characteristics of small amplitude electromagnetic waves propagation at different altitudes in the ionosphere. These waves have been studied by many authors (see for example Fejer [1960], Thompson [1963], or Bostick [1964]). It is well established that the following simplifications may be made when treating electromagnetic propagation above 100 km.

i) displacement current may be neglected

ii) pressure terms may be neglected

iii) ions are positive and singly charged.

The usual derivation of the propagation characteristics of plane waves, in a plasma with a magnetic field present, will now be outlined. First the current $\vec{J}$ is related to the electric field $\vec{E}$ through the conductivity tensor σ. If the magnetic field is parallel to the x_3 axis of an x_1, x_2, x_3 coordinate system, the relation between $\vec{J}$ and $\vec{E}$ is (see Thompson [1963])

$$\begin{pmatrix} J_{x_1} \\ J_{x_2} \\ J_{x_3} \end{pmatrix} = \begin{pmatrix} \sigma & \sigma_x & 0 \\ -\sigma_x & \sigma_\perp & 0 \\ 0 & 0 & \sigma_o \end{pmatrix} \begin{pmatrix} E_{x_1} \\ E_{x_2} \\ E_{x_3} \end{pmatrix} \qquad 2.2.1$$

where

σ_o is the parallel conductivity

$\sigma_\perp$ is the perpendicular conductivity

σ_x is the Hall conductivity.

Assuming $e^{-i\omega t}$ time dependence, suitable expressions for the conductivities are given as (see Francis and Karplus [1960])

$$\sigma_o = N_e e^2 \frac{1}{m_e (\nu_e - i\omega)}$$

$$\sigma_\perp = N_e e^2 \left\{ \frac{\nu_e - i\omega}{n_e[(\nu_e - i\omega)^2 + \omega_e^2]} + \frac{\nu_i - i\omega}{n_i[(\nu_i - i\omega)^2 + \omega_i^2]} \right\} \qquad 2.2.2$$

$$\sigma_x = N_e e^2 \left\{ \frac{-\omega_e}{n_e[(\nu_e - i\omega)^2 + \omega_e^2]} + \frac{\omega_i}{n_i[(\nu_i - i\omega)^2 + \omega_i^2]} \right\}$$

where ω_e is the electron gyro frequency $\simeq 8. \times 10^6$ rad/sec

ω_i is the ion gyro frequency

$\simeq 2. \times 10^2$ rad/sec at 100 to 600 km altitude

$\simeq 2. \times 10^3$ rad/sec at 1000 km altitude

N_e is the electron number density

ν_e is the electron collision frequency, equal to the sum of the the electron-ion and the electron-neutral collision frequencies

ν_i is the ion-neutral collision frequency

m_e and m_i are the electron and ion masses.

Madden and Thompson (1964) have expressed $\sigma_\perp$ and σ_x in a convenient form, which gives numerical values which agree with the values given by the expressions 2.2.2 to within factors on the order of $\frac{m_e}{m_i}$. Their expressions are

$$\sigma_\perp \simeq \sigma_o \frac{1 + W\Omega}{(1+W^2)(1+\Omega^2)}$$

$$\sigma_x \simeq \sigma_o \frac{W}{(1+W^2)(1+\Omega^2)} \qquad 2.2.3$$

where

$$W = \frac{\omega_e}{\nu_e - i\omega}$$

$$\Omega = \frac{\omega_i}{\nu_i - i\omega} \qquad 2.2.4$$

Now that the conductivity tensor has been obtained, it is combined with Maxwell's equations to find the propagation constant for plane waves in the ionosphere. Let η be a unit vector in the direction of propagation and let γ be the angle η makes with the magnetic field. If k is the propagation constant of the wave, the space dependence of the field quantities is $e^{ik\eta}$. Inserting this space dependence into Maxwell's equations

$$\nabla \times \vec{H} = \vec{J}$$

$$\nabla \times \vec{E} = i\omega \vec{B} \qquad 2.2.5$$

and relating $\vec{E}$ to $\vec{J}$ by equation 2.2.1 leads to a dispersion relation

$$F(k, \gamma, \omega) = 0$$

For fixed γ and ω this equation has two roots for k^2. The expressions for these roots are quite complicated in the general case. Fortunately, for altitudes above 100 km, because σ_o is greater than 10^4 times as large as $\sigma_\perp$ or σ_x, a comparatively simple approximation for the roots can be used in a discussion of the propagation. This approximation, called the quasi-longitudinal approximation, is valid when the condition $\sigma_o \cos^2 \gamma \gg \sigma_\perp \sin^2 \gamma$ is satisfied (see Madden and Thompson [1964]).

This condition is only invalid very close to $\gamma = 90^{\circ}$. The quasi-longitudinal approximation is

$$k^2 \simeq \frac{i\mu\omega\,\sigma_\perp}{2}\left[\left(1 + \frac{1}{\cos^2\gamma}\right) \pm \sqrt{\left(1 - \frac{1}{\cos^2\gamma}\right)^2 - \left(\frac{\sigma_x}{\sigma_\perp}\right)^2 \frac{4}{\cos^2\gamma}}\right] \qquad 2.2.6$$

Let the roots corresponding to the plus and minus signs in this expression be denoted respectively by k_f^2 and k_g^2. When $\gamma = 90^{\circ}$, i.e., propagation is perpendicular to the magnetic field, the propagation constants are given by (see Thompson [1963]) as

$$k_f^2 = i\mu\omega\left[\sigma_\perp + \frac{\sigma_x^2}{\sigma_\perp}\right] \qquad 2.2.7$$

$$k_g^2 = i\mu\omega\left[\sigma_o\right] \qquad 2.2.8$$

In Table 2.2-1 values of Ω and W are given for several heights. These values are based on the following: $\omega = .6$ rad/sec; $\omega_i = 2. \times 10^2$ rad/sec; $\omega_e = 8 \times 10^6$ rad/sec; with ν_e and ν_i taking the values given in Table 2.1-1.

TABLE 2.2-1

W and Ω versus height

Height km	W Pure Number	Ω Pure Number
100	1×10^2	.07
130	2×10^3	3.
160	8×10^3	30.
200	1×10^4	80. + 20i
320	1×10^4	7. + 30i
450	2×10^4	1. + 30i

Above 100 km $W \gg 1$ and therefore expressions 2.2.3 give the ratio of σ_x to $\sigma_\perp$ as

$$\frac{\sigma_x}{\sigma_\perp} = \frac{W}{1 + W\Omega} \cong \frac{1}{\Omega} \qquad 2.2.9$$

This expression, together with the values of Ω in table 2.2-1, shows that the Hall conductivity is not important above approximately 140 km, but is important from 100 km to 130 km.

Above 140 km, σ_x may be neglected in expression 2.2.6; the propagation constants, for γ not very close to 90°, are then given by

$$k_f^2 = k_\perp^2 \qquad 2.2.10$$

$$k_g^2 = k_\perp^2 / \cos^2 \gamma \qquad 2.2.11$$

where $k_\perp^2 \equiv i\mu\omega\sigma_\perp$

$$\cong \frac{\mu N_e m_i}{B_o^2} (\omega^2 + i\omega\nu_i)$$

The root designated as k_f^2 is associated with the fast or unguided wave type. k_f^2 is independent of γ and so the propagation is isotropic. The other root, k_g^2, is associated with the guided Alfven wave. Notice that when $\nu_i \ll \omega$, which is true above 400 km, both wave types have real propagation constants and so propagate with little damping.

For $\gamma = 90^\circ$, since σ_o is large and real, expression 2.2.8 shows the guided wave type to be highly attenuated. Above 140 km, σ_x may be neglected, and expression 2.2.7 shows $k_f^2 \cong k_\perp^2$ for $\gamma = 90^\circ$.

2.3 Discussion of Wave Type Coupling

In this section we will consider coupling between the fast and guided wave types. The models studied in chapters III and IV are special cases, because the geometry of these models is such that the fast wave type propagates with no coupling to the guided wave type.

In the following it is shown that for the lower order modes of the real cavity there should be little coupling between the fast and the guided wave types. Therefore, the conclusions drawn from the models studied in chapters III and IV should not be invalid, because no wave type coupling occurs in these models.

In the ionosphere the physical properties change much more rapidly in the vertical directions than in the horizontal directions. Therefore, to analyze the coupling between wave types it is appropriate to consider a model which is stratified parallel to the earth's surface. The earth's curvature will be neglected and so the analysis will be carried out in rectangular geometry. The continuous variation of the properties in the vertical direction may be replaced by a series of homogeneous layers. In each layer, either wave type will propagate independently of the other. However, at the boundaries between the layers coupling between the wave types can occur.

To show that the coupling between wave types which occurs at the boundaries between the layers should not be great we will demonstrate that the horizontal components of the electric fields of the two wave types will be almost perpendicular and that the horizontal components

of the magnetic fields of the two wave types will also be almost perpendicular.

Let us consider a rectangular coordinate system in which the x, y, and z axes are, respectively, the south, east, and upward vertical directions. In a particular layer the magnetic field and the plasma are uniform. The magnetic field is in the x, z plane and dips at an angle ψ below the -x axis. We make the approximations that σ_o is infinite, and σ_x is zero. In the last section these approximations were shown to be valid above 140 km. The region of the ionosphere below 140 km will be considered in the next sec

Let the space dependence of the waves be of the form

$$\{\exp i(k_x x + k_y y + k_z z)\} \qquad 2.3.1$$

With this space dependence, E_z and the three components of $\vec{H}$ can be eliminated from Maxwell's equation. We are left with a pair of homogeneous linear equations for E_x and E_y. Details of this procedure can be found in a paper by Nishida (1964). In the limit of infinite σ_o and zero σ_x the two linear equations are

$$E_x\left(\frac{k_y^2}{\sin^2\psi} + k_z^2 + 2k_x k_z \cot\psi + k_x^2\cot^2\psi - \frac{k_\perp^2}{\sin^2\psi}\right) + E_y(-k_x k_y + k_x k_y \cot\psi) = 0$$

2.3.2

$$E_x(k_y k_z \cot\psi - k_x k_y) + E_y(k_x^2 + k_z^2 - k_\perp^2) = 0$$

Since σ_o is infinite, the electric field must be perpendicular to the main magnetic field. Therefore

$$\frac{E_z}{E_x} = - \cot \Psi \qquad 2.3.3$$

To match boundary conditions on the horizontal planes separating the layers, both the fast and guided wave types must have the same horizontal wave numbers. These wave numbers may still be denoted by k_x and k_y. Let the vertical wave numbers for the fast and guided wave types be denoted by $k_{z,f}$ and $k_{z,g}$. For equations 2.3.2 to have nonzero solutions, the three wave numbers for each wave type must obey a dispersion relation. The dispersion relations for the two wave types are

$$k_{z,f} = \left[k_\perp^2 - k_x^2 - k_y^2 \right]^{1/2} \qquad \text{fast} \qquad 2.3.4$$

$$k_{z,g} = \frac{1}{\sin \Psi} \left[\pm k_\perp - k_x \cos \Psi \right] \qquad \text{guided} \qquad 2.3.5$$

We now show that the wave propagation, at a frequency near the Pc 2,3 resonance, is close to vertical for both wave types. Let $\lambda_{z,f} = \frac{2\pi}{k_{z,f}}$; $\lambda_{z,f}$ is the vertical wave length of the fast wave type. $\frac{1}{4} \lambda_{z,f}$ is comparable to the cavity height. As was discussed in section 1.3, the cavity height is under 1000 km. Therefore, we see that $\lambda_{z,f} < 4000$ km. The longest horizontal wave length possible is the circumference of the earth ($\cong$ 40,000 km); this distance is 10 times $\lambda_{z,f}$. Therefore, for the longer horizontal wave lengths, i.e., low order modes, the propagation is close

to vertical. From this, we have for the fast wave type

$$\left| k_{z,f} \right| \gg k_x,\ k_y \qquad 2.3.6$$

Equation 2.3.4 gives

$$k_\perp \geq \left| k_{z,f} \right|$$

so

$$k_\perp \gg \left| k_x \right|,\ \left| k_y \right|$$

$$\left| \frac{1}{\sin \psi}\ k_\perp \right| \gg \left| k_x \right|,\ \left| k_y \right|$$

Neglecting $k_x \cos \psi$ in comparison to $k_\perp$, we have from this inequality and equation 2.3.5

$$\left| k_{z,g} \right| \cong \left| \frac{1}{\sin \psi}\ k_\perp \right| \gg \left| k_x \right|,\ \left| k_y \right| \qquad 2.3.7$$

So we have shown that propagation is close to vertical for both wave types.

The ratios of E_y to E_x are given by equation 2.3.2 as

$$\frac{E_y}{E_x} = \frac{k_y k_{z,f} \cot \psi - k_x k_y}{k_y^2} \qquad \text{fast} \qquad 2.3.8$$

$$\frac{E_y}{E_x} = - \frac{k_y k_{z,g} \cot \psi - k_x k_y}{(k_{z,g} \cos \psi - k_x \sin \psi)^2} \qquad \text{guided}$$

For mid-latitude we may assume $\cot \psi \cong 1$. Then considering the inequalities 2.3.6 and 2.3.7 the field ratios are approximately

$$\left.\begin{aligned} \frac{E_y}{E_x} &\cong \frac{k_{z,f}}{k_y} \cot \psi \qquad \text{fast} \\ \frac{E_y}{E_x} &\cong - \frac{k_y}{k_{z,g} \sin \psi \cos \psi} \qquad \text{guided} \end{aligned}\right\} \quad 2.3.9$$

Using Maxwell's equation $\nabla \times \vec{E} \cong i \mu \omega \vec{H}$, the components of $\vec{H}$ can be obtained from the components of $\vec{E}$ for each wave type. If the component E_x is normalized to 1, the vector fields of the two wave types are written

$$\left.\begin{aligned} \vec{E} &\cong \left(1, \frac{k_{z,f}}{k_y} \cot \psi, - \cot \psi\right) \\ \vec{H} &\cong \frac{1}{\mu\omega} \left(-k_y \cot \psi - \frac{k_{z,f}^2}{k_y} \cot \psi, k_{z,f} - k_x \cot \psi, \frac{k_x k_{z,f}}{k_y} \cot \psi - k_y\right) \end{aligned}\right\} \text{fast} \quad 2.3.10$$

$$\left.\begin{aligned} \vec{E} &\cong \left(1, - \frac{k_y}{k_{z,g} \sin \psi \cos \psi}, - \cot \psi\right) \\ \vec{E} &\cong \\ &\frac{1}{\mu\omega} \left(-k_y \cot \psi - \frac{k_y}{\cos \psi \sin \psi}, k_{z,g} - k_x \cot \psi, - \frac{k_x k_y}{k_{z,g} \cos \psi \sin \psi} - k\right) \end{aligned}\right\} \text{guided} \quad 2.3.11$$

We wish to show clearly the dominant components of the field vectors given in expressions 2.3.10 and 2.3.11. To do this we will let Λ be a measure of the magnitude of any one of the four ratios $(k_{z,f}/k_x)$, $(k_{z,f}/k_y)$, $(k_{z,g}/k_x)$, or $(k_{z,g}/k_y)$. Λ will be much greater than 1 for long horizontal wave lengths. We again assume that $\cot \psi \cong 1$. Then the magnitude of the components in terms of Λ, for larger Λ, are written

$$\vec{E} \cong (1, \Lambda, 1)$$

$$\vec{H} \cong \frac{k_y}{\mu\omega} (\Lambda^2, 1, \Lambda) \qquad 2.3.12$$

$$\vec{E} \cong (1, 1/\Lambda, 1)$$

$$\vec{H} \cong \frac{k_y}{\mu\omega} (1, \Lambda, 1)$$

The horizontal components of the fast mode are a predominantly eastward electric field and a northward magnetic field. The horizontal components of the guided wave are predominantly northward for the electric field and eastward for the magnetic field. From this we see the horizontal components are almost perpendicular and so little coupling occurs.

2.4 Effect of the Hall Conductivity

The models to be studied in this thesis cover a region from the earth's surface to 1000 km altitude. There is a region between approximately 70 km and 140 km where the Hall conductivity is significant in determining the wave propagation constants (see section 2.3). The Hall conductivity has not been included in the models to be studied in this

thesis even though it is significant in determining the wave propagation constants in a part of the region covered by these models.

In this section we explain why the Hall conductivity has not been included in each of the two models. In addition we will access the effect which excluding the Hall conductivity will have on the results obtained using the models.

The Hall conductivity has been excluded from the daytime model to be studied in chapter III for the following reason. In this model when the Hall current is neglected a solution can be obtained by solving a scalar partial differential equation. This solution has only an eastward component of the electric field. If the Hall conductivity is included, the other components of the electric field will be introduced. If the other components of the electric field are present it will be necessary to solve a vector wave equation. This would greatly increase the difficulty of obtaining the solution.

Let us consider the extent to which the solutions to the two-dimensional model studied in chapter III will be modified by the exclusion of the Hall conductivity. We will do this by examining one-dimensional solutions. Prince, Bostick, and Smith (1964) have made computations for plane wave propagation which show that the resonant frequency is not affected greatly by the Hall region and that little wave coupling occurs in this region. We will discuss some of their results. They considered a layered model for daytime conditions with a horizontal magnetic field. The incoming waves were of the fast type. The computation

was first made with the model extending down to the surface, then repeated with the Hall region excluded by terminating the model with a perfect conductor at 130 km. The resonant frequency was within 5 per cent in the two cases. This result may be interpreted as an indication that the resonant frequency is determined above the Hall region.

In the terminated case the Q of the resonant peak was higher than it was for the model extending down to the earth's surface. However, results of Li et al. (1964) show that much of this increase of Q is due to the removal of the air layer rather than to the removal of the Hall region. The effect of the air layer is also considered in appendix I.

Prince, Bostick, and Smith (1964) also considered an incoming vertically propagating wave of the fast type in a daytime model with the magnetic field dipping at 60°. The propagation was in the north-south-vertical plane. In this case some coupling between the fast and guided wave types was found to occur in the Hall region. A study was made of the coupling for a frequency of .085 cps. The authors found almost all the coupling occurred below 200 km. This would be expected, since the Hall current is very small above that height. The reflected fast wave was 10 times as large as the reflected guided wave, showing that the wave type coupling resulting from the Hall conductivity is not large.

In the daytime model studied in chapter IV, as in the daytime model of chapter III, the Hall conductivity has been neglected. In the chapter IV daytime model propagation is always perpendicular to the direction of the main magnetic field. Under this condition expression 2.2.8 shows that

only the fast mode propagates. The guided mode will not be excited even if the Hall conductivity is present. Because of this, the problem can still be solved as a scalar partial differential equation when the Hall conductivity is included. Madden (1964) developed a method for solving this problem by the use of network analogies. There is, however, a difficulty in applying the method to the present problem. A term in the partial differential equation which governs this problem, when the Hall conductivity is included, contains the partial derivatives of σ_x with respect to position. Near 100 km σ_x changes very rapidly with height and it is difficult to handle the $\frac{\partial \sigma_x}{\partial r}$ term numerically.

A second complication that arises in the daytime model of chapter IV from the Hall term is seen if we examine k_f. Let α and β be respectively the real and imaginary parts of k_f, and let $\hat{\phi} = \tan \frac{\beta}{\alpha}$ be the phase angle of k_f. In Table 2.4-1 values of α and β for several values of γ have been taken from daytime model values given by Prince, Bostick, and Smith (1964). The phase angle, $\hat{\phi}$, at 100 km has also been given.

When $\hat{\phi} \cong 90^\circ$, the wave propagation is evanescent, which means that even though the amplitude of a wave decreases in the direction of propagation, no energy is dissipated. When $\hat{\phi} \cong 45^\circ$, energy is dissipated as the wave progresses. It is at approximately 100 km that $|k_f|$ is greatest. At this height we see that $\hat{\phi} \cong 45^\circ$ only for γ close to 90°, i.e., when the propagation is almost perpendicular to the main magnetic field. In the model of chapter IV this is the case. Therefore a considerable amount of damping is introduced by the Hall conductivity. Because

TABLE 3.4-1

Real and Imaginary Parts of k_f

(values from Prince, Bostick, and Smith [1964])

$$k_f = \alpha + i\,\beta$$

α and β in units of $(km)^{-1}$

$$B_o = .5 \text{ Gauss}$$

γ / Altitude	0^o		30^o		60^o		85^o		90^o	
	$\alpha x 10^2$	$\beta x 10^2$	$\alpha x 10^2$	$\beta x 10^2$	$\alpha x 10^2$	$\beta x 10^2$	$\alpha x 10^2$	$\beta x 10^2$	$\alpha x 10^2$	$\beta x 10^2$
90. km	.0065	.24	.007	.26	.010	.34	.19	.73	.72	.72
100.	.088	1.6	.10	1.7	.16	2.2	1.8	5.0	3.4	3.4
110.	.33	1.6	.38	1.8	.59	2.3	1.9	1.9	1.9	1.9
120.	.65	.12	.70	1.3	1.3	1.3	1.1	1.1	1.1	
130.	.62	.81	.69	.85	.74	.75	.73	.74	.73	
	$\hat{\phi}$		$\hat{\phi}$		$\hat{\phi}$		$\hat{\phi}$		$\hat{\phi}$	
$\hat{\phi}$ at 100 km	87^o		87^o		86^o		70^o		45^o	

propagation is almost vertical in the low velocity Hall region, only at the magnetic equator, in the actual ionosphere, is the propagation perpendicular to the magnetic field. If σ_x is included in the model the amount of damping will be typical of only a small region around the equator.

The values of k_f which were given by the daytime model presented in section 2.1 are shown in Table 2.4-2. When these values were computed σ_x was set to be zero. Therefore $k_f = i \mu \omega \sigma_\perp$.

TABLE 2.4-2

Real and Imaginary Parts of $i \mu \omega \sigma_\perp$

$\sigma_x = 0$

$i \mu \omega \sigma_\perp = \alpha + i \beta$

α and β in units of $(km)^{-1}$

Altitude \ γ	$B_o \cong .3$ Gauss		$B_o \cong .5$ Gauss	
	0^o		60^o	
	$\alpha \times 10^2$	$\beta \times 10^2$	$\alpha \times 10^2$	$\beta \times 10^2$
100 km	.25	.25	.23	.23
130	.94	.94	.86	.86

It may be seen that at 130 km altitude the values of k_f given in Table 2.4-2 are similar to those of Table 2.4-1. However, the values of k_f in Table 2.4-2 are much smaller, at 100 km, than the values in Table 2.4-1. The high dissipation at the equator due to the Hall conductivity is no longer present.

As was noted, the resonant frequency of the oscillations is determined above the Hall region, so the resonant frequencies given by the model of chapter IV will be accurate.

Thus far we have studied the effects of excluding the Hall region in the daytime models studied in chapters III and IV. Under nighttime conditions $|k_f|$ is always less than $(30 \text{ km})^{-1}$. Since the region where the Hall conductivity is important is only 30 km thick, under nighttime conditions, the region is too thin to have any important effect on the waves.

CHAPTER III

SPHERICAL MODEL FOR STUDY OF LONGITUDE INDEPENDENT PROPAGATION

3.1 Outline of Chapter III

In this chapter models are studied in which all quantities are independent of longitude. Using this type of model, we consider the effect of the horizontal variation due to a dipole magnetic field on the resonances of the cavity below the high Alfven velocity region.

In section 3.2 the model is described and the governing partial differential equation is derived.

In section 3.3 the region covered by the solution is described and boundary conditions are formulated.

In section 3.4 an idealization of the model is discussed. This is done to give the reader insight into the form of the resonant modes and also to introduce mode notation.

In section 3.5 a few matters pertaining to the solution are discussed. The majority of the work of solving the mathematical model is not covered in this section. It can be found in Appendix II.

In section 3.6 the results of the computation are presented and discussed with reference to the observed characteristics of the Pc 2,3 oscillations.

3.2 Description of Model and Derivation of the Partial Differential Equation

In this section an equation is obtained which governs the solution for longitude independent propagation of the fast wave type in the earth's ionosphere. The approach employed is similar to the one used by Dungey (1954) to treat magnetohydrodynamic motion. In the present work, however, the electromagnetic, rather than the magnetohydrodynamic point of view is taken. This is done to enable us to include the effect of ion-neutral collisions in the expression for the propagation constant.

Consider a spherical coordinate system in which r, ϕ, and θ are respectively the radius, longitude, and co-latitude. In the present model the ionospheric parameters are symmetric about the polar axis. The magnetic field of the earth is represented by a dipole field of the dipole moment $M_d = 8.07 \times 10^{15}$ in mks. The strength of this magnetic field is then $|B_o| = \frac{M_d}{r^3} \sqrt{1 + 3\cos^2\theta}$. The dipole axis coincides with the axis of the coordinate system. The solutions studied will be symmetric about this axis. Therefore, $\frac{\partial}{\partial \phi} = 0$ for all quantities involved in the equations. Furthermore, the cross conductivity σ_x is neglected (see section 2.4). Under these conditions a two-dimensional partial differential equation for E_ϕ may be found. Maxwell's equations are

$$\nabla \times \vec{H} = \vec{J} + \vec{S} = \sigma \vec{E} + \vec{S} \qquad 3.2.1$$

$$\nabla \times \vec{E} = i \mu \omega \vec{H} \qquad 3.2.2$$

where S is a current source.

These equations combine to give

$$\nabla \times \nabla \times \vec{E} = i \mu \omega (\sigma_\perp \vec{E} + \vec{S}) \qquad 3.2.3$$

Since the ϕ direction is perpendicular to the dipole magnetic field the ϕ component of the current $\vec{J}$ is simply $\sigma_\perp E_\phi$, where $\sigma_\perp$ is the perpendicular conductivity given in expression 2.2.2. Remembering that $\frac{\partial E_\phi}{\partial \phi} = 0$, the ϕ component of 3.2.3 is given by

$$-r^{-2} \frac{\partial}{\partial \theta} \sin^{-1} \frac{\partial}{\partial \theta} \sin \theta \, E_\phi - r^{-1} \frac{\partial}{\partial r^2} r E_\phi = k_r^2 E_\phi + i \mu \omega S_\phi \qquad 3.2.4$$

where $k_r^2 = i \mu \omega \sigma_\perp$.

Equation 3.2.4 does not contain E_r or E_θ, and the r and θ components of 3.2.4 can be solved for E_ϕ, since the equation for the other components of the electric field are uncoupled. The waves satisfying 3.2.4 are of the fast or unguided type, since they propagate isotropically and the electric vector is perpendicular to both the dipole field, $\vec{B}_o$, and the direction of propagation. It is now convenient to introduce the variables

$$\psi = r \sin \theta \, E_\phi$$

and

$$x = \cos \theta$$

and write equation 3.2.4 as

$$\left[\frac{1}{(1-x^2)}\ \frac{\partial^2}{\partial r^2} + r^{-2}\frac{\partial^2}{\partial x^2} + \frac{k_f^2}{(1-x^2)}\right]\Psi = \omega g \qquad 3.2.5$$

where

$$g = \frac{i\mu S_\phi}{(1-x^2)} \qquad 3.2.6$$

3.3 Boundary Conditions

In figure 3.3-1 the region for which a solution will be found is shown in r,θ coordinates; in figure 3.3-2 the corresponding region of the r,x plane is shown. The boundaries are labeled to show how they are mapped from the r,θ plane to the r,x plane. Only the solutions to equation 3.2.5, which are symmetric about the equator, were studied; thus, the solution need only be obtained for the northern hemisphere. Therefore, the equator is a boundary of the region. The region extends from the earth's surface at 6380 km to the outer boundary at radius r_m. In the models studied, r_m is 12,380 km which is several thousand km higher than the top of the resonating cavity.

The unionized region below the ionosphere is represented by a layer, having the propagation constant of free space. This air layer extends from the earth's surface to 100 km altitude. The earth's surface is treated as a perfect conductor; the justification for this approximation is given by Nishida (1964).

FIG. 3.3-1

SOLUTION REGION IN r,θ PLANE

BOUNDARIES DENOTED BY B_1, ETC.

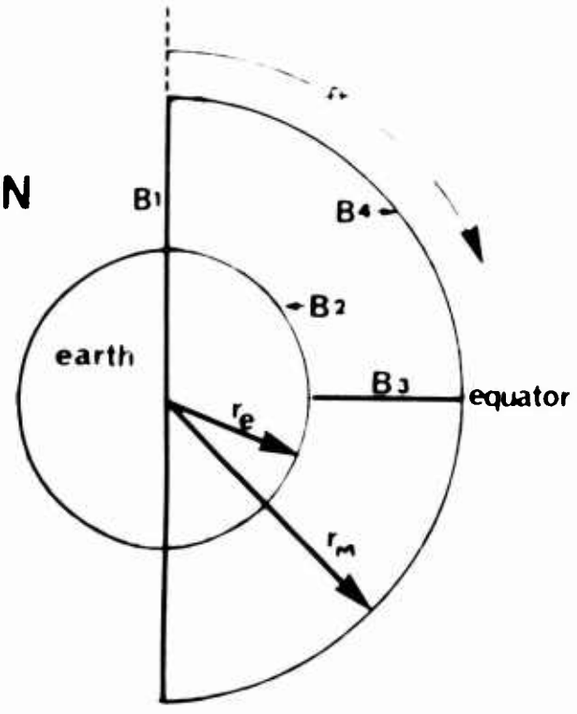

FIG. 3.3-2

SOLUTION REGION IN r,x PLANE

BOUNDARIES DENOTED BY B_1, ETC.
NOTE CORRESPONDENCE WITH FIG. 3.3-1

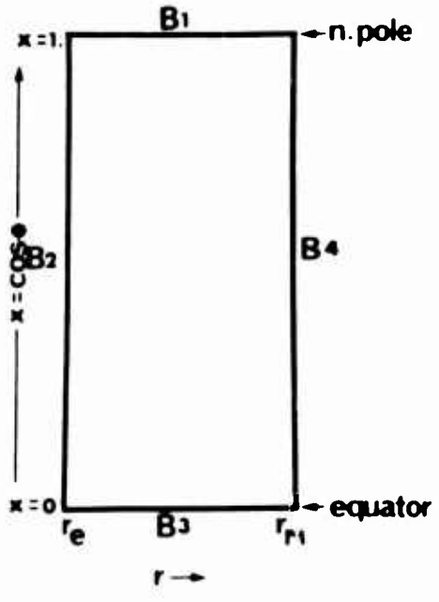

ψ obeys the following boundary conditions:

On boundary B1: For E_ϕ to be finite the boundary condition on $\psi = r \sin\theta E_\phi$ must be $\psi = 0$.

On boundary B2: $E_\phi = 0$ on the earth's surface. Therefore $\psi = 0$.

On boundary B3: for solutions symmetric about the equator $\frac{\partial \psi}{\partial x} = 0$.

On boundary B4: on this boundary the boundary condition is not as straightforward as on the other boundaries. When analytical solutions to the wave equation are obtained for bounded regions, a radiation condition is imposed which separates energy originating from sources in the region from that coming in from outside the region. (See Courant and Hilbert[1962], p. 315)

In this thesis the equation 3.2.5 will be solved numerically rather than analytically. Therefore, it was necessary to formulate a local boundary condition analogous to the radiation condition. Sources were included interior to boundary B4; for this reason a boundary condition was chosen which would assure an outward flow of energy at boundary B4. The boundary condition which was used on the boundary B4 was that waves will be outgoing and will travel in the direction of the outward normal to surfaces of equal Alfven velocity v_a.

We now show how this boundary condition is imposed. In figure 3.3-3 a point in boundary B4 is shown. Let E_{ϕ_p} be the value of E_ϕ at a point p on the boundary and let ξ be the distance measured in the direction of the outward normal. Then, the behavior of a wave traveling along the outward normal is written

FIG. 3.3-3
GEOMETRY FOR
BOUNDARY B4

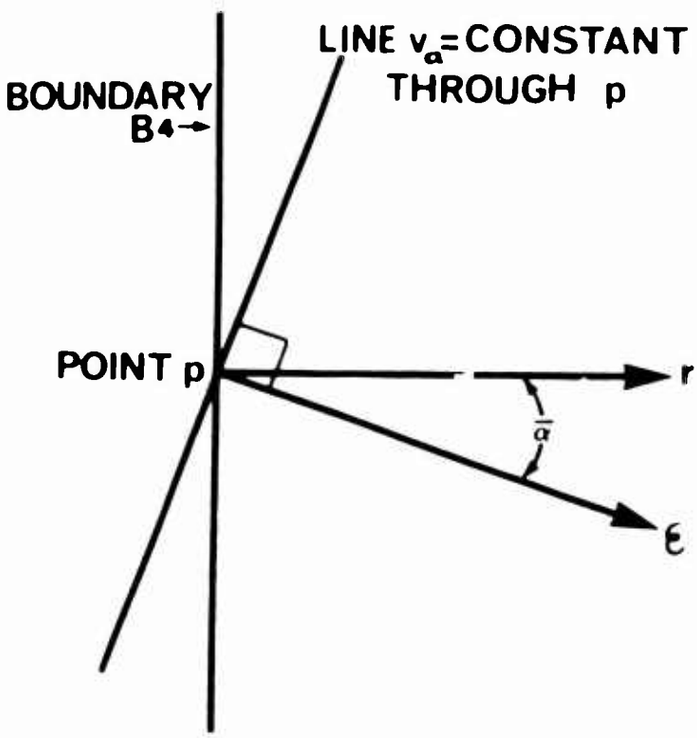

$$E_\phi = E_{\phi_p} \exp\{i \xi k_f\} \qquad 3.3.1$$

$$\frac{\partial E_\phi}{\partial \xi} = i k_f E_\phi \qquad 3.3.2$$

Let $\bar{\alpha}$ be the angle between the direction of propagation and the outward normal, $\cos \bar{\alpha}$ is found from

$$\cos \bar{\alpha} = - \frac{(\nabla v_a) \cdot \vec{r}}{|\nabla v_a| \, |\vec{r}|} \qquad 3.3.3$$

The radial derivative of E_ϕ is given by

$$\frac{\partial E_\phi}{\partial r} = \frac{\partial E_\phi}{\partial \xi} \cos \bar{\alpha} \qquad 3.3.4$$

Equations 3.3.2 and 3.3.4 are combined with the definition of ψ to give the boundary condition on B4

$$\frac{\partial \psi}{\partial r} - \left[\frac{1}{r} + i k_f \cos \bar{\alpha} \right] \psi = 0 \qquad 3.3.5$$

3.4 Mode Structure and Notation

At this point a discussion of the mode structure in a two-dimensional region, which is greatly simplified representation of the situation in the

ionosphere, will be helpful in interpreting the solutions of equation 3.2.5. The homogeneous part of equation 3.2.5 is of the form

$$A \frac{\partial^2 V}{\partial y^2} + B \frac{\partial^2 V}{\partial r^2} + C\ V = 0 \qquad 3.4.1$$

If both A and B are positive, equation 3.4.1 is termed an elliptic partial differential equation. Now, A and B, as well as C, in equation 5 are positive throughout the region of interest; they are also positive for the scalar wave equation

$$\frac{\partial^2 V}{\partial y^2} + \frac{\partial^2 V}{\partial r^2} + k^2 V = 0 \qquad 3.4.2$$

$$k^2 = \frac{\omega^2}{v^2} = \left(\frac{2\pi f}{v}\right)^2$$

where v is the propagation velocity and f the wave frequency.
It is expected, then, that the solutions of the wave equation will have some points of similarity with those of equation 3.2.5. Since they are simple to visualize, we will consider the solutions of the wave equation for a constant velocity region. The region under consideration is idealized as a rectangle (see figure 3.4-1). L_r represents the altitude at which the top of the cavity reflects the trapped energy, and not the boundary of the model B4. V is analogous to $\psi = E_\phi r \sin\theta$ of equation 3.2.5. Therefore, suitable boundary conditions on V are the following. On the side representing the poles, at $y = 0$ and $y = L_y$,

FIG. 3.4-1
RECTANGULAR SOLUTION REGION

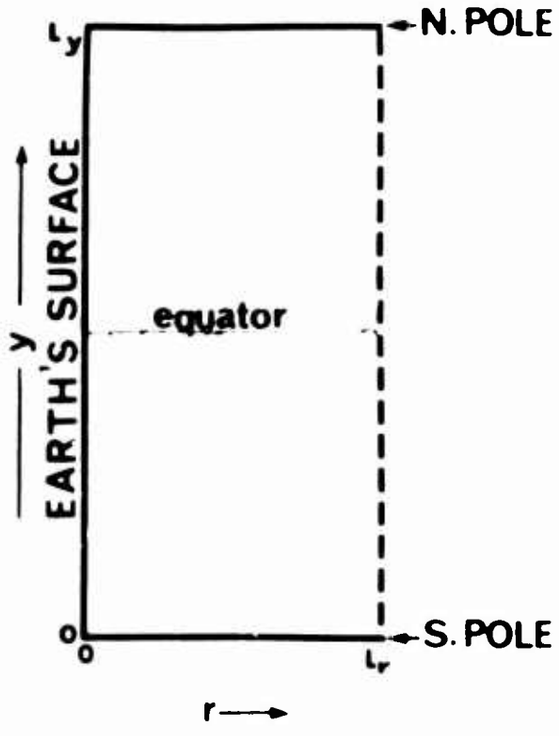

and on the earth's surface, V = 0. In the idealization of infinite velocity at $r = L_r$ the condition on the boundary, at $r = L_r$, is $\frac{\partial V}{\partial r} = 0$. Then the eigen solutions to the equation 3.4.2, for this region, are

$$\sin k_m r \quad \sin k_n y \qquad 3.4.3$$

with

$$k_m = \frac{\pi}{2L_y} (2m-1)$$

$$k_n = \frac{\pi n}{L_y}$$

$$k^2 = k_m^2 + k_n^2$$

The vertical mode number is m and the horizontal number is n. The resonant frequencies which are real are given by

$$f_{m,n} = \frac{v}{2\pi} \left[k_m^2 + k_n^2 \right]^{1/2} \qquad 3.4.4$$

To give some feeling for the differences between the resonant frequencies of the lower modes let us take values that very roughly typify the cavity region. The region extends much further in the horizontal than in the vertical direction. Let

$$v = 300 \text{ km/sec}$$

$$L_y = 15{,}000 \text{ km}$$

Two values are used for L_r to show how the height of the cavity affects the difference in the resonant frequency between successive modes. We see from the discussion in section 1.3 that it is probable that 750 km rather than 1500 km is the more realistic value for L_r. The lower resonant frequencies from equation 3.4.3 are given in Table 3.4-1.

TABLE 3.4-1

Mode Resonant Frequencies

		$f_{m,n}$ (cps)	
m	n	L_r = 750 km	L_r = 1500 km
1	1	.1004	.0510
1	2	.1016	.0538
1	3	.104	.0583
1	5	.111	.0689
2	1	.3002	.1503

From this table we see that the frequencies of the m = 2 mode is a factor of 3 greater than the resonant frequencies of the m = 1 modes. For the m = 1 modes the resonant frequency increases with n, but these changes of frequency are much smaller than the difference between the resonant frequencies of the m = 1 and m = 2 modes. This change with m is small because for a short, wide region the wave fronts are close to vertical. The percentage of change in resonant frequency between the

$m = 1$, $n = 1$ mode and the $m = 1$, $n = 5$ mode is 11 per cent when $L_r = 750$ km and 35 per cent when $L_r = 1500$ km. The percentage of change is greater for the large value of L_r.

For the modes for which n is odd the solutions are symmetric about the equator; for the even n the solutions are antisymmetric. It is the modes for which n is odd and $m = 1$ that will be investigated in the computations.

3.5 Matters Pertaining to the Solution of the Model

In the section just completed an idealized model was discussed in terms of the eigen functions of the region. This is not the approach which we have chosen to use in studying the resonances in the cavity of the two-dimensional model of the real ionosphere. Our approach is to excite the cavity with harmonic sources and to observe the response as the frequency of the source is varied.

It was found necessary to employ finite difference techniques to solve equation 3.2.5. A thorough discussion of the application of these techniques to the present problem has been placed in appendix II. The solutions obtained are in terms of the variable $\psi = E_\phi r \cos\theta$. The magnetic field is obtained numerically from ψ using the Maxwell's equation $\nabla \times \vec{E} = i\omega \vec{B}$.

A given source distribution will excite more than one mode of the cavity. If the modes have high Q's or if there are large differences in their resonant frequencies, the observed response near a particular mode's resonant frequency will be almost entirely due to that mode. Neither of these conditions is met for the modes under investigation. Therefore

it is possible for a considerable amount of mode mixing to occur in the cavity.

To enable us to circumvent the problem of mode mixing when examining the character of individual modes, source distributions were used which excited a particular mode to a much greater extent than they excited any other mode. The notation used to describe the source distributions exciting the individual modes is D1 for the n = 1 mode of the daytime model, N1 for the n = 1 mode of the nighttime model, etc. These source distributions are given in appendix II.

3.6 Discussion of Results

Nighttime and Daytime Model Results and Effect of Variation of k_f with Latitude

The nighttime model was excited successively with source distributions N1, N3, and N5. The three modes n = 1, 3 and 5 for m = 1 were observed.

For the three modes, the surface variation of B_θ^2, as a function of $x = \cos\theta$, has been plotted in figure 3.6-1. For each mode, B_θ^2 was plotted for a frequency, f, close to that mode's resonant frequency. The values of B_θ^2 for the three modes have been adjusted by arbitrary factors to allow them to be plotted on the same figure. This figure shows that the n = 1 mode has no nodes between the equator and the pole, while the n = 3 and n = 5 modes have 1 and 2 respectively. This is in agreement with the mode structure given for the idealized case discussed in section 3.4. The two maxima of the n = 3 mode are of nearly the same amplitude as the three maxima of the n = 5 mode.

Figure 3.6-1

Variation of B_n^2 with Latitude, Night Model

3 Modes

B_n^2 plotted for a frequency, f, close to the resonant frequency of each mode

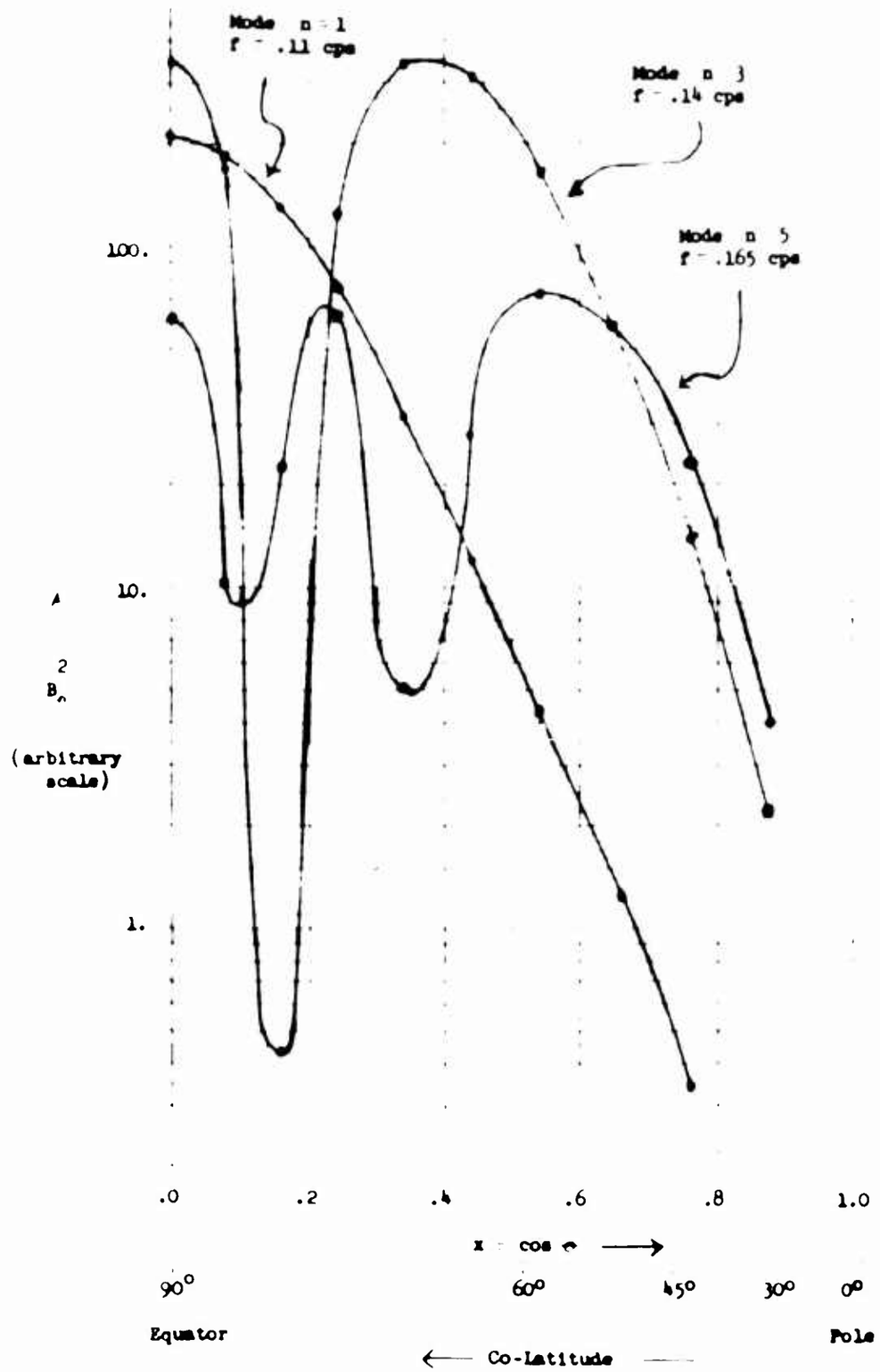

The variation of the response with frequency for the three modes was studied by plotting B_θ^2, divided by B_θ^2 at the resonant frequency, at a fixed point on the surface for each mode. The surface point used for each mode was the point at which that mode had its maximum amplitude. This frequency response is shown in figure 3.6-2. The resonant frequencies are .110, .143, and .162 cps for the n = 1, 3 and 5 modes. These correspond to periods of 9.1, 7.0, and 6.2 sec. There is a difference of 30 per cent between the n = 1 and n = 3 resonant frequencies and of 47 per cent between the n = 1 and n = 5 resonant frequencies.

The daytime model was treated in the same manner. The excitations which were used were the daytime source distributions given in appendix II. In figure 3.6-3 the surface values of B_θ^2 are given. The variation of B_θ^2 with x was clear for the n = 1 and n = 3 modes. The n = 1 mode shape for the daytime model is similar to that of the nighttime n = 1 mode. The n = 3 mode has one node between the equator and the pole as did the nighttime n = 3 mode. However, the maxima at the equator is much smaller than the other maxima. When the D5 sources were run the other modes were excited to a sufficient extent to mask the mode response at low latitudes. This has been indicated by the dotted line in figure 3.6-3.

The response as a function of frequency for the modes of the daytime model are shown in figure 3.6-4. The resonant frequencies are .058, .077, and .087 for the n = 1, 3 and 5 modes. The corresponding periods are 17.5, 13.0, and 11.5 sec. For the daytime model there is a difference of 30 per cent between the n = 1 and n = 3 resonant frequencies and of 47 per cent between the n = 1 and n = 5 resonant frequencies.

Figure 3.6-2

B_{ϕ}^2 vs. Frequency, Night Model

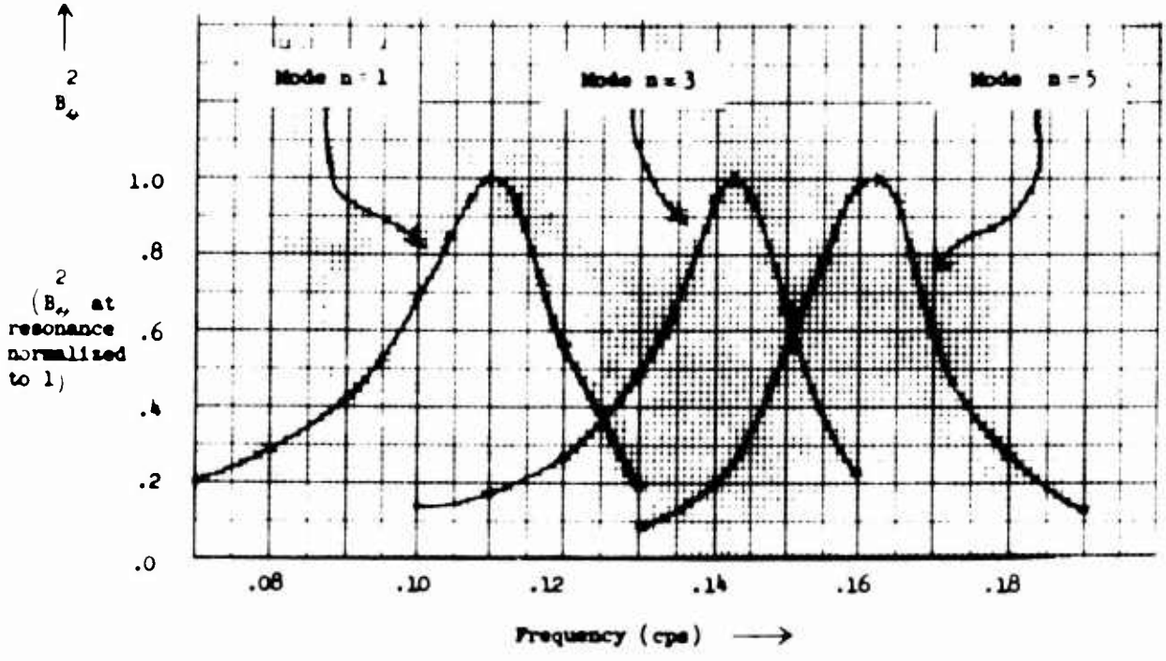

Figure 3.6-3

Variation of B_θ^2 with Latitude, Day Model

3 Modes

B^2 plotted for a frequency, f, close to the resonant frequency of each mode

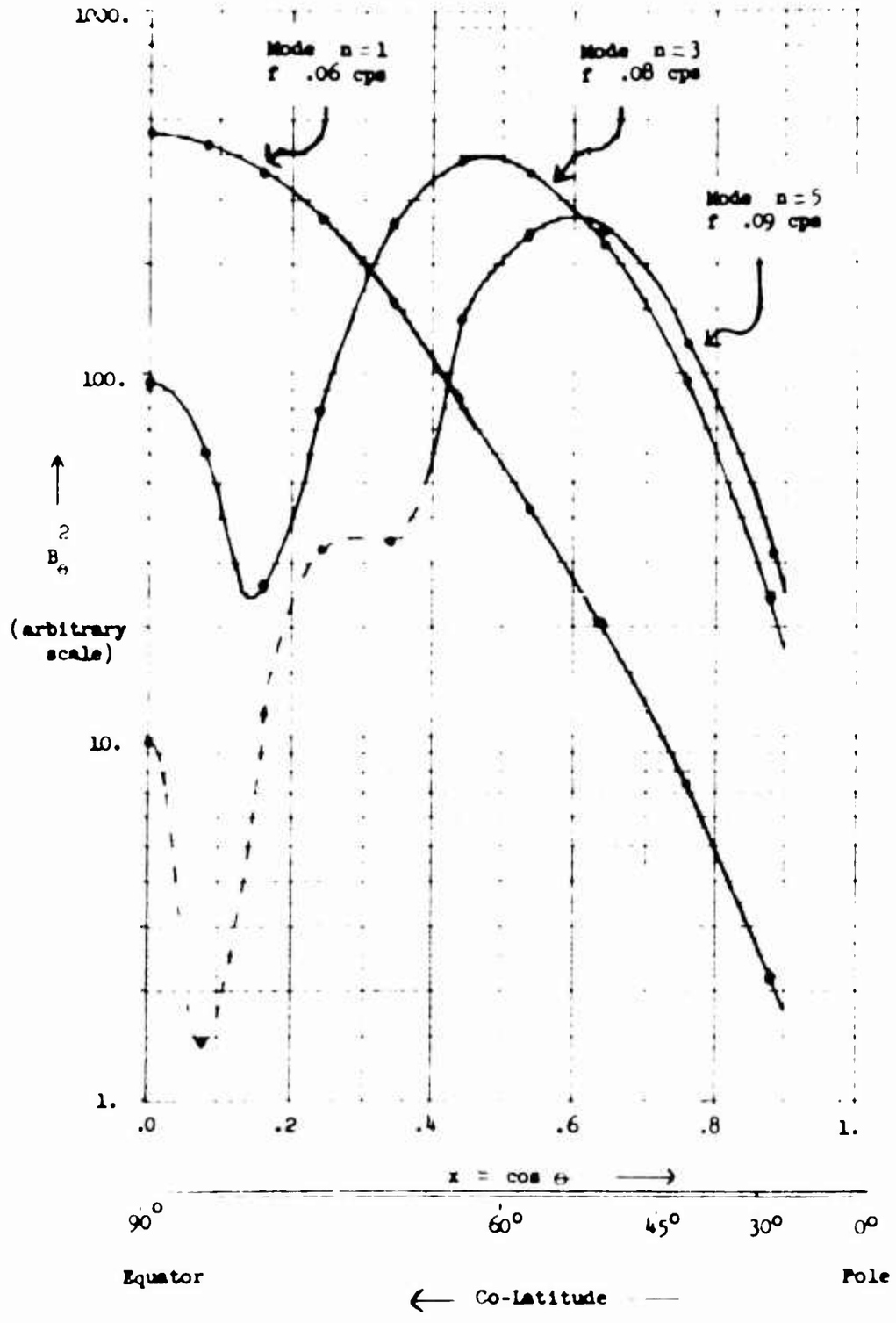

Figure 3.6-4

B_ϕ^2 vs. Frequency, Day Model

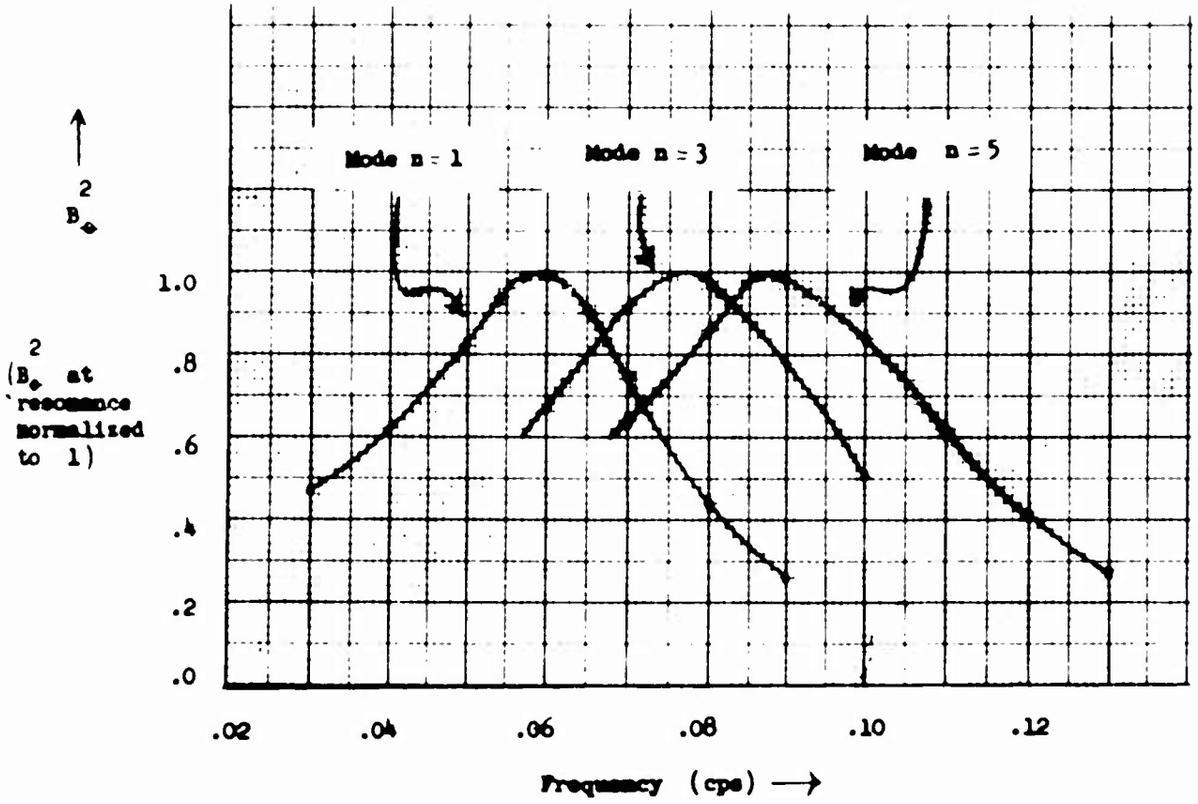

These results show that a significant difference exists between the resonant frequencies of the n = 1, 3 and 5 modes for both the day and night models. This difference is greater than that given by either of the constant velocity rectangular models of section 3.4. As was stated, the model with a height L_r = 750 km is probably a more realistic model of the cavity; the change for this model from the n = 1 to the n = 5 mode was only 11 per cent.

We wish to investigate whether these differences in the mode resonant frequencies result mainly from geometric considerations or from the decrease of k_f with latitude resulting from the increase of the dipole magnetic field strength with latitude. To do this computations were carried out with a model in which the magnetic field strength had no latitude dependence. The strength of the field at all latitudes was equal to the equatorial dipole strength $\frac{M_d}{r^3}$. Thus k_f is a function of r, only.

Computations were carried out using the daytime model with the D1, D3, and D5 sources. For each source the resonant frequencies were approximately .058. The uncertainty in the resonant frequencies is perhaps .003 cps. The uncertainty results because the n = 1, 3 and 5 modes all have almost the same resonant frequency and more mode mixing occurred than in the dipole field case. This result indicates that the change of resonant frequency between modes is due almost entirely to the variation of k_f with latitude. For the nighttime model excited by the N1 source distribution the resonant frequency was .105 cps.

For both the day and night models, run with the dipole magnetic field, the resonant frequency of the n = 1 mode is close to the resonant frequency found when the magnetic field had the equatorial value at all latitudes. This indicates that it is the conditions at the equator that determine the resonant frequency of the n = 1 mode.

This fact can explain the daytime Pc 3 periods of close to 20 seconds which are observed at mid-latitude. It is difficult to explain periods this long in terms of plane wave models which have a mid-latitude magnetic field. Li et al (1964) made calculations for the model with a daytime ionospheric model similar to the one used in this thesis and obtained a period of only 12 seconds.

Let us consider the manner in which the electron density must be increased to explain this difference between the observed periods and that predicted by the plane wave model. The Alfven velocity is proportional to $\sqrt{\frac{1}{N_e}}$. The period should be proportional to $\sqrt{\frac{1}{v_a}}$. If the electron density profile goes up uniformly by a factor C, we may predict that the period will increase by a factor $\sqrt{C}$. This prediction is supported by a comparison of the periods of the n = 1 modes of the day and night models, and the use of $N_m F_2$ as a measure of the electron densities of the two models. The ratio of the periods of the day and night models is $\frac{17.5}{9.1} = 1.9$. The square root of the ratio of the daytime to the nighttime model value of $N_m F_2$ (see section 2.1) is $\sqrt{\frac{2.1 \times 10^6}{.4 \times 10^6}} = 2.3$.

To raise the period from the 12 sec, given by the mid-latitude field layered model, to the observed periods of 20 seconds, the daytime electron density profile must be raised by a factor of 2.8. In the resulting model $N_m F_2$ would be increased to a value of 5.9×10^6 electrons/cc. This value is much higher than any observed. It is, therefore, difficult to explain the observed mid-latitude periods using layered models in which the propagation constant is independent of horizontal position. In the two-dimensional model the 17.5 sec period of the n = 1 mode is close to the observed period and only a modest adjustment in the electron density is necessary to reach agreement with the observed periods.

Damping Effects from Ion-Neutral Collisions

The values of ν_i used in the daytime model were computed from a low neutral density model. Results in this section will show that the resonant frequency of the model is not changed to any significant degree by changes of ν_i in the model. The Q of the resonant peak, however, will be seen to be dependent on the value of ν_i used. Two models were used to examine the effect of varying $\sigma_\perp$ in the lower ionosphere. In the MCFD model the collision frequencies ν_i have higher values from 200 to 370 km than the values which were used in the daytime model. Over most of this height range $\sigma_\perp$ is almost pure real and proportional to ν_i. Therefore, increasing ν_i should increase the dissipation.

The second model, the MEPM model, has lower values of N_e in the ionosphere below 280 km. Since $\sigma_\perp$ is proportional to N_e, in this model, $\sigma_\perp$ is smaller in the lower ionosphere and less dissipation may be expected.

Figure 3.6-5

B^2 vs. Frequency for 3 Models

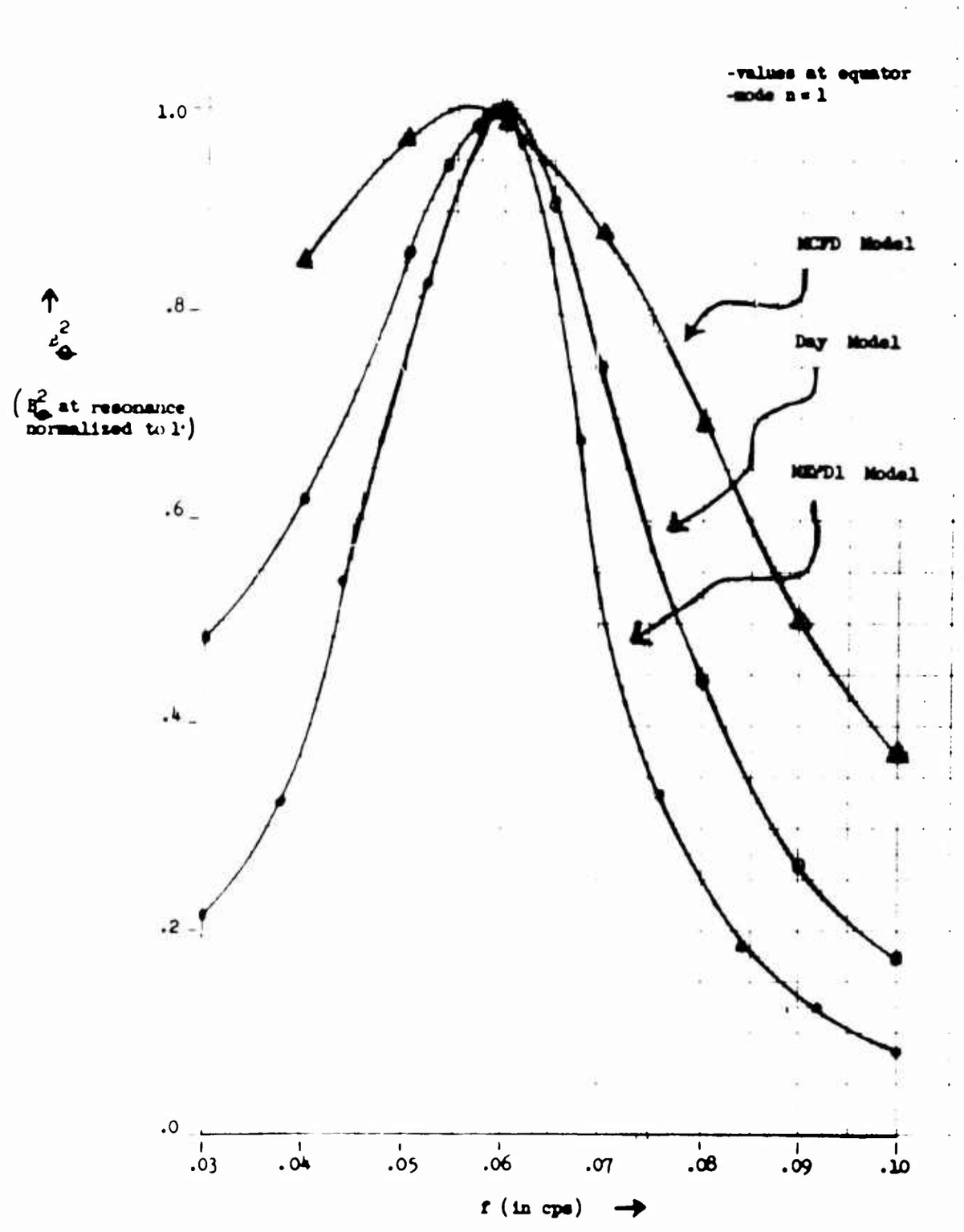

Computations were carried out with these two models and the unmodified daytime model using the D1 source distribution to excite the n = 1 mode. In figure 3.6-5 the value of B_θ^2 at the equator is plotted versus frequency for each model. The resonant frequencies of the basic daytime model and the MEPD1 model are approximately .058 cps, while the MCFD model has a resonant frequency of approximately .056 cps. Therefore, the increased damping in the MCFD model caused only a 3 per cent change, from the value found with the daytime model, in the frequency of the n = 1 mode. A change of approximately 3 per cent was also found for the n = 3 mode. These results indicate that the resonant frequency is almost independent of the damping which occurs below 400 km. From this we may conclude that the resonant frequencies found with the daytime model should not be significantly in error even if the collision frequencies in the model are too low.

The Q of the MEPD1 model is 2.4. For the daytime model Q = 1.4. The peak obtained with the MCFD mode is too flat to obtain a value of Q. The Q of the cavity is seen to be very dependent on the values taken by σ_1 in the lower ionosphere.

In the lower ionosphere σ_1 varies greatly with latitude and longitude, as well as with height. Energy dissipation will occur throughout the lower ionosphere. To get meaningful values for Q a more complete model for the ionosphere than the one used in the present work will be needed.

Effect of Locally Perturbed Electron Density

Computations were carried out with the MEPD2 model. In this model the electron density has values somewhat higher than the daytime values in the region covering latitudes 14^{o} to 26^{o} and the height range of 240 to 1000 km. The model was excited with the D1, D3, and D5 source distributions. The solutions were very similar to those obtained through the use of daytime model. The resonant frequencies were slightly lower for each mode, but the decrease in resonant frequency was less than .003 cps for each mode.

Results with Localized Source Distributions

It is of interest to see the response to source distributions which are confined to a small range of latitude. Two source distributions were used with the daytime ionospheric model.

First, low latitude sources, located between the equator and 9^{o} latitude, were used. The source distribution used is given in appendix II. With this source distribution the apparent resonant frequency at all latitudes was .058 cps, the resonant frequency of the n = 1 mode. The variation of B_{θ}^{2} with latitude was very similar to the variation resulting from excitation with the D1 source distribution. It is concluded that the modes other than the n = 1 mode were not excited to any significant extent.

The second local source investigated was located between 39.5^{c} and $49.^{o}$ latitude. The exact description of this source is given in appendix II.

When the model is excited by this source, the largest response occurs at the latitude of the source. At this latitude the resonant frequency is between .09 and .10 cps. This frequency is higher than the resonant frequency of the n = 5 mode, but this source is at a higher latitude than the latitude at which the n = 5 mode has its maximum response. It may be the n = 7 mode which has been most strongly excited by this source. The frequency at which the maximum response occurs decreases with latitude. At the equator the resonant frequency is close to .06, which is approximately the resonant frequency of the n = 1 mode. The daytime results showed that the n = 1 mode was the only one with a large response at low latitudes. Therefore, it is probably the n = 1 mode which is being seen at the equator even though the source did not strongly excite this mode.

CHAPTER IV

CYLINDRICAL MODEL FOR STUDY OF EAST-WEST LATITUDE-INDEPENDENT PROPAGATION

4.1 Description of the Model and Derivation of the Partial Differential Equation

In this section we derive the equation governing propagation in a cylindrical coordinate system. The coordinates are, r, λ, and z. The model geometry is shown in figure 4.1-1. λ is the longitude relative to the sum which is located at $\lambda = 0^{o}$, i.e., $\lambda = 0^{o}$ at noon and 180^{o} at midnight. The main magnetic field is parallel to the z axis. The strength of the magnetic field of the model is the value $\frac{8.07 \times 10^{15}}{r^3}$, which represents the magnetic field strength in the earth's equatorial plane.

$$\frac{1}{r}\frac{\partial H_z}{\partial \lambda} - \frac{\partial H_\lambda}{\partial z} = \sigma_\perp E_r \qquad 4.1.1$$

$$\frac{\partial H_z}{\partial r} - \frac{\partial H_r}{\partial z} = \sigma_\perp E_\lambda \qquad 4.1.2$$

$$\frac{1}{r}\frac{\partial}{\partial r}(r H_r) - \frac{1}{r}\frac{\partial H_r}{\partial \lambda} = \sigma_o E_z \qquad 4.1.3$$

$$\frac{\partial r E_\lambda}{\partial r} - \frac{\partial E_r}{\partial \lambda} = i r \mu \omega H_z - S_z \qquad 4.1.4$$

$$\frac{1}{r}\frac{\partial E_z}{\partial \lambda} - \frac{\partial E_\lambda}{\partial z} = i \mu \omega H_\perp \qquad 4.1.5$$

FIG. 4.1-1
GEOMETRY FOR CHAPTER IV MODEL

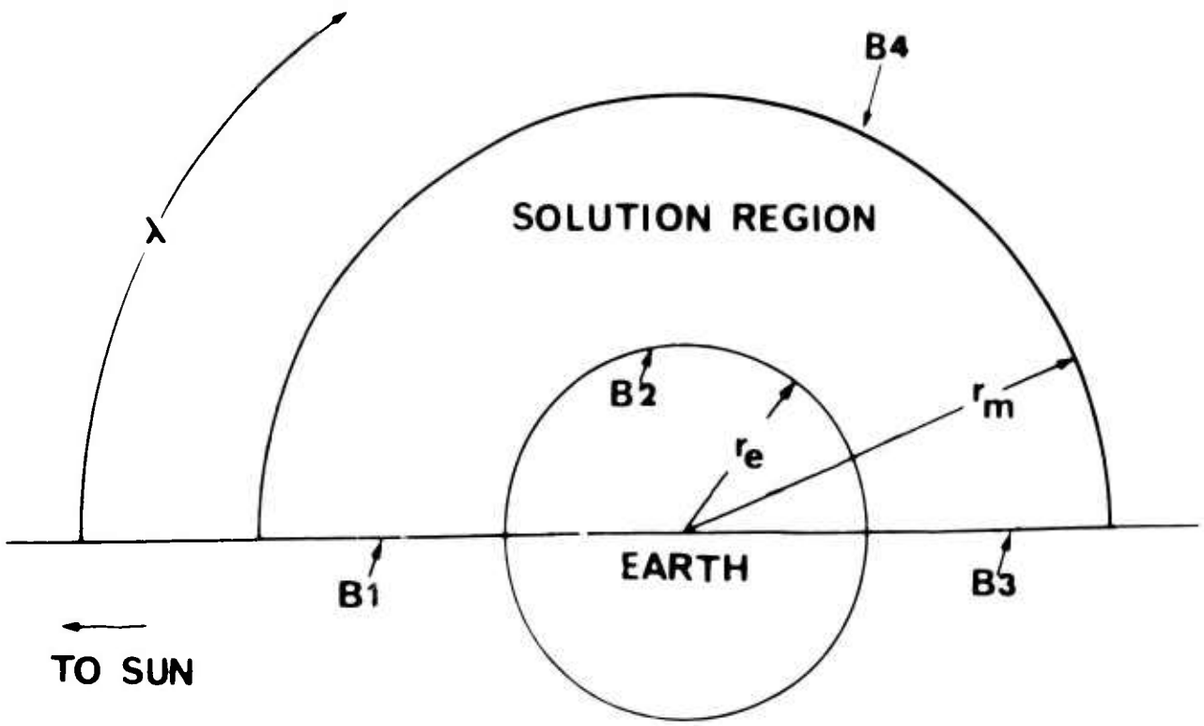

$$\frac{\partial E_r}{\partial z} - \frac{\partial E_z}{\partial r} = i\mu\omega H_\lambda \qquad 4.1.6$$

where S_z is the source term.

In this model solutions which are independent of z propagate around the cylinder and travel perpendicular to the main magnetic field lines. This type of propagation is a model for east-west propagation around the earth at low latitudes.

If the solutions are independent of z, equations 4.1.1 to 4.1.6 separate into two sets; one set contains only H_z, E_r, and E_λ, while the other set contains only H_λ, H_r, and E_z. The waves governed by the second set of equations are very highly damped in the ionosphere, because E_z is parallel to the main magnetic field. It is the waves governed by the first set of equations which will be studied. These are waves of the fast wave type.

A difficulty arises when the propagation is completely independent of z. Since the magnetic field of the wave is transverse to the direction of propagation, the results of appendix I show that the magnetic field at the surface will be almost completely destroyed. The difficulty can be avoided by the introduction of a small z dependence of the form $e^{ik_z z}$ into the solutions. With this z dependence equations 4.1.1 to 4.1.6 are not strictly uncoupled. The coupling which does exist, however, is very small. The following analysis shows that it will be possible to neglect the coupling between the equations.

In the ionosphere σ_o, the parallel conductivity, is very large. Thus E_z will be small. From 4.1.5 and 4.1.6 we then have

$$\begin{cases} \dfrac{\partial H_r}{\partial z} \cong k_z^2 \dfrac{1}{i\mu\omega} E_\lambda \\ \dfrac{\partial H_\lambda}{\partial z} \cong -k_z^2 \dfrac{1}{i\mu\omega} E_r \end{cases} \qquad 4.1.7$$

Putting equations 4.1.7 into equations 4.1.2 and 4.1.1 gives

$$\frac{1}{r} \frac{\partial H_z}{\partial \lambda} \cong \sigma_e E_r \qquad 4.1.8$$

$$\frac{\partial H_z}{\partial r} \cong - \sigma_e E_\lambda \qquad 4.1.9$$

where

$$\sigma_e = \left(\sigma_\perp - \frac{k_z^2}{i\mu\omega} \right)$$

may be considered the effective conductivity.

A value of $k_z = 5 \times 10^{-7}$ km^{-1} was used in the computations. Then k_z^2 is small compared with $|i\mu\omega\sigma_\perp|$ in the ionosphere and can be neglected.

In the air layer, located between the earth's surface and 100 km altitude, the conductivity is isotropic and has the value $\sigma_a = -i\omega\epsilon_o$. Since the value of E_z is very small in the ionosphere and at the surface $E_z = 0$, E_z must be very small throughout the layer. Thus it follows that

4.1.7 is applicable in the air layer. In 4.1.8 $|i\mu\omega\sigma_a|$ is not much larger than k_z^2 and is in fact considerably smaller for the value of k_z used. The effective conductivity in the atmosphere is

$$\sigma_e = \sigma_a - \frac{k_z^2}{i\mu\omega}$$

It is then possible to combine equations 4.1.4 and 4.1.8 to obtain a partial differential equation governing the behavior of H_z.

$$\frac{\partial}{\partial r}\left(r\,\frac{1}{\sigma_e}\,\frac{\partial H_z}{\partial r}\right) + \frac{\partial}{\partial \lambda}\left(\frac{1}{r\sigma_e}\,\frac{\partial H_z}{\partial \lambda}\right) + i\mu\omega\, r\, H_z - S_z = 0 \qquad 4.1.10$$

This equation is valid in both the ionosphere and in the air layer.

4.2 Region of Solution and Boundary Conditions

Equation 4.1.10 is solved in the region shown in figure 4.1-1. Solutions are constrained to be symmetric about the earth-sun line. Therefore, only the region $0 \leq \lambda \leq 180^\circ$ is considered.

The boundary conditions on the boundaries shown in figure 4.1-1 are as follows:

On the boundaries B1 and B3: the symmetry around the earth-sun line gives $\frac{\partial H_z}{\partial \lambda} = 0$.

On boundary B2: because the earth may be treated as a perfect conductor, $E_\lambda = 0$ on B2. Equation 4.1.9 then gives the boundary condition in terms of the H_z as $\frac{\partial H_z}{\partial r} = 0$.

On boundary B4: sources have been included inside the region.

To simulate a radiation condition we establish the boundary condition that waves of the fast type must be flowing radically outward on boundary B4. This may be expressed mathematically in the following manner. Near a boundary point, p

$$H_z = H_{z_p} e^{ik_f(r-r_m)}$$

this gives the homogeneous boundary condition

$$\frac{\partial H_z}{\partial r} - ik_f H_z = 0 \qquad 4.2.1$$

on B4.

4.3 Variation of Ionospheric Parameters with Position

In the model studied in this chapter the parameters of the ionosphere are functions of λ as well as r. Let $\epsilon(r,\lambda)$ represent any one of the ionospheric parameters: electron density, ion mass, electron collision frequency, or ion collision frequency. The value of this parameter at any position is given by

$$\epsilon(r,\lambda) = [1 - G(\lambda)] \cdot \epsilon_D(r) + [G(\lambda)] \cdot \epsilon_N(r)$$

In this formula $\epsilon_D(r)$ and $\epsilon_N(r)$ are the values of the parameter which are given by the daytime and nighttime models, respectively, in section 2.1. $G(\lambda)$ is a function which gives the manner in which the parameters of the model change from their daytime to their nighttime values. $G(\lambda)$ is the same for each parameter. It is shown vs. λ in figure 4.3-1.

Figure 4.3-1

Plot of $G(\lambda)$ vs. λ

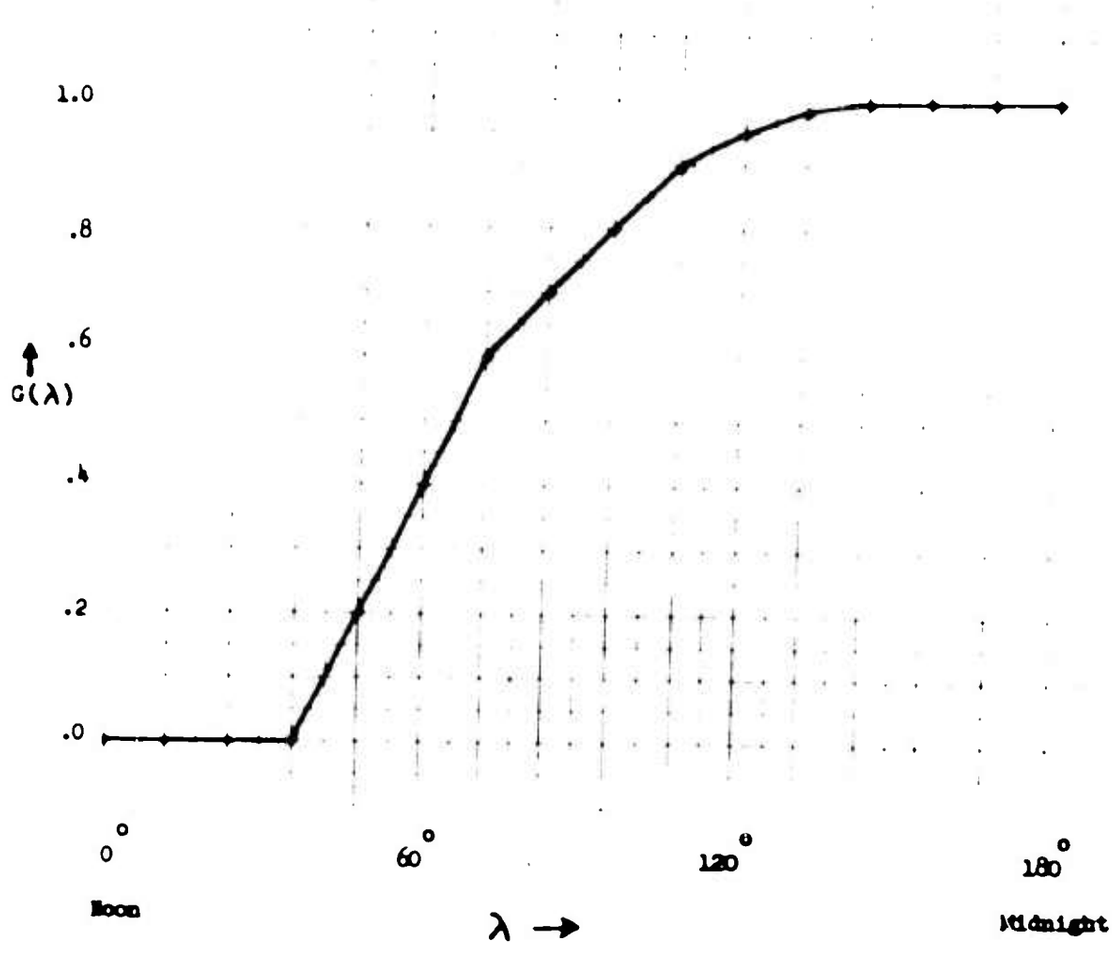

4.4 Method of Solution of Equation 4.1.10

The solution of equation 4.1.10 in the region shown in figure 4.1-1 was obtained by the use of finite difference methods. The details of the procedure are described in appendix III.

4.5 Discussion of Results

Source Distributions

The response to two source distributions was investigated. In the first source distribution, the sources had uniform strength for all values of λ. The second source distribution represents subsolar sources. The sources in this distribution have their maximum value under the sun ($\lambda = 0^{o}$) and the values decrease to zero at $\lambda = 72^{o}$. The strength of the sources in these two distributions as a function of λ is given in figure 4.5-1. The altitude of the sources was 2000 km.

Uniform Source Distribution

Let us first discuss the computations made for the uniform source distribution. In figure 4.5-2 the value of B_z^2 at the surface is plotted against λ for a number of frequencies. The apparent resonant frequency at a fixed position on the surface is the frequency at which the response is greatest. In figure 4.5-3 the apparent resonant frequencies and the corresponding periodsare plotted against λ. For the uniform source distribution the resonant period appears to vary with local time in a manner similar to the ionospheric model. This diurnal variation of period may be compared with the variation, given by Kato and Saito (1959), shown in figure 1.2-1

Figure 4.5-1

Source Strength as a Function of λ

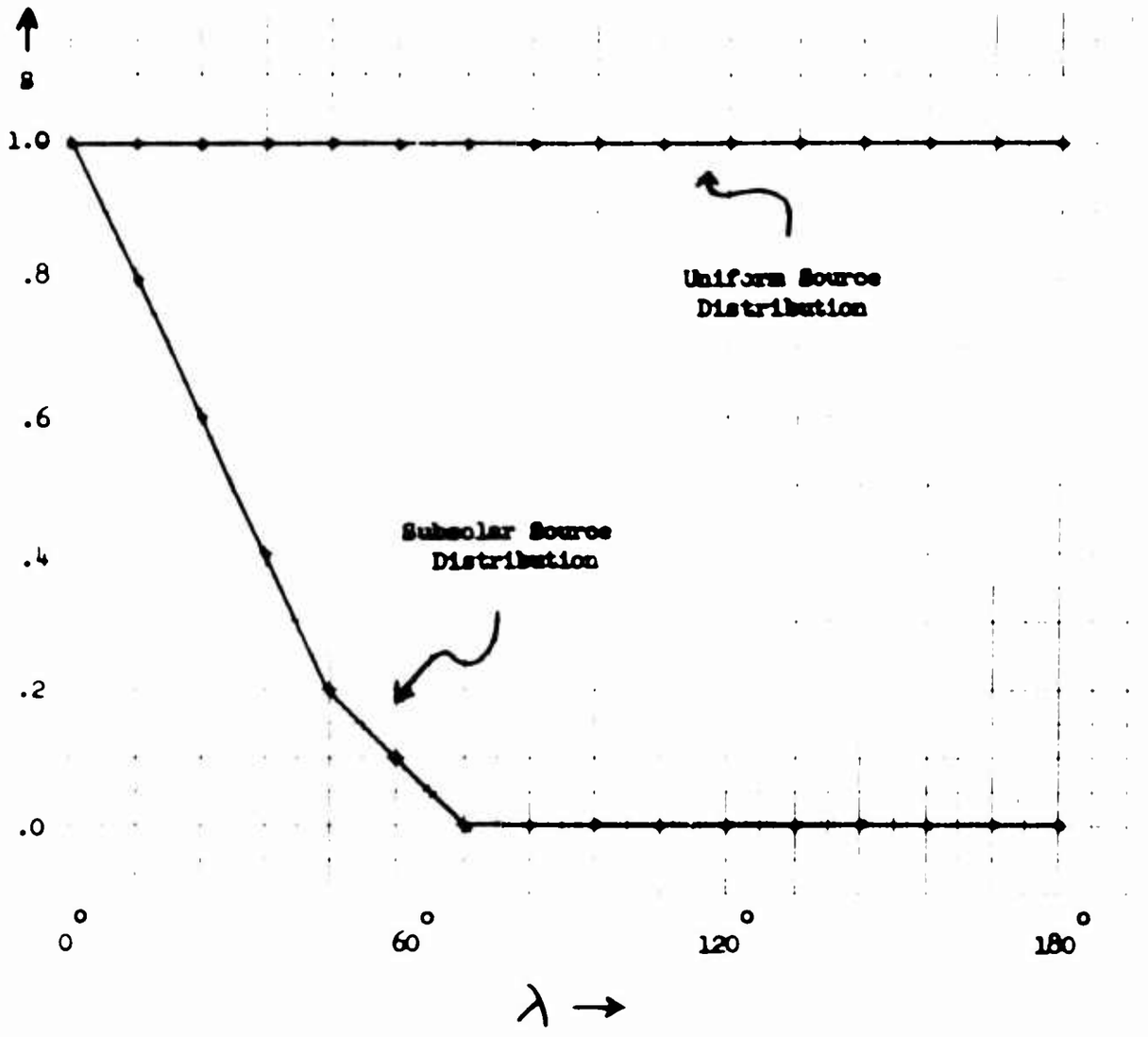

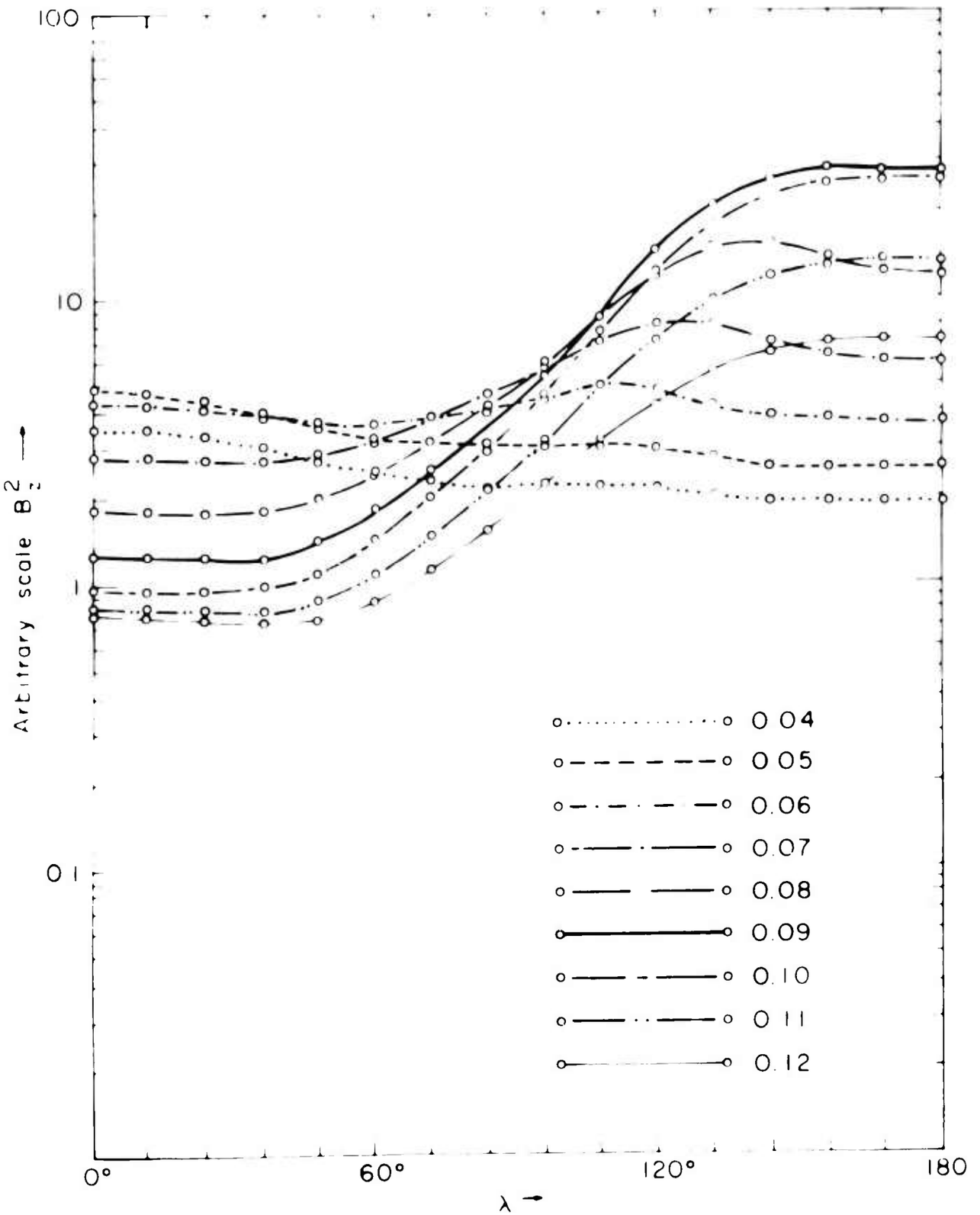

Figure 45-2 Plot of B_z^2 on surface vs λ

Plotted for several values of frequency

UNIFORM SOURCE DISTRIBUTION

Figure 4.5-3

Plot of Resonant Frequency vs. λ,

for Uniform Source

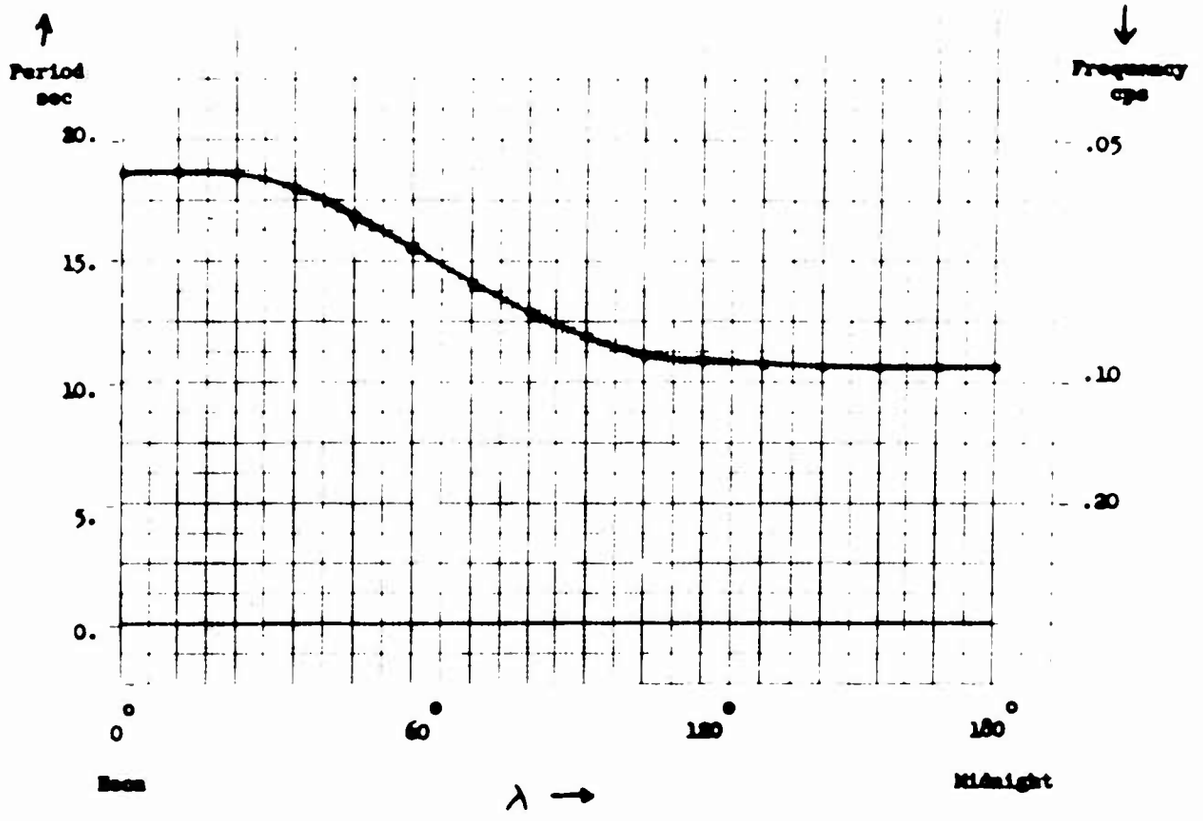

Subsolar Source Distribution

The results of the case when the model was excited with the subsolar source distribution will now be discussed. In figure 4.5-4 the value of B_z^2 as a function of λ has been plotted for a number of frequencies. This figure shows the noon resonant period to be .054 which is similar to the period given by the uniform source distribution. The resonant frequency increases with λ, from $\lambda = 0^o$ to approximately $\lambda = 130^o$. The amplitude of the response is much smaller in the nighttime than in the daytime. These results show that a source in the daytime hemisphere will not greatly excite oscillation in the nighttime hemisphere.

The model studied in this chapter is one for which the transport of energy from one hemisphere to the other is relatively easy. This is so because propagation is nearly east-west and because the change from daytime to nighttime conditions is gradual, so that in this model no sharp boundary exists between the day and night hemispheres. Therefore, since the model, when excited by subsolar sources, shows oscillations having much greater amplitude in the day than in the night hemisphere, in the real ionosphere a subsolar source should excite micropulsations, which would be confined mainly to the day hemisphere.

Observations of micropulsations show that the level of activity is much higher during the day than at night; the greatest level of activity occurs during the hours around local noon. Two of the possible sources of micropulsations should be most active near noon: the thermally excited motion of the neutral atmosphere and the interaction of the solar wind with magnetosphere boundaries. If the major sources for Pc 2,3

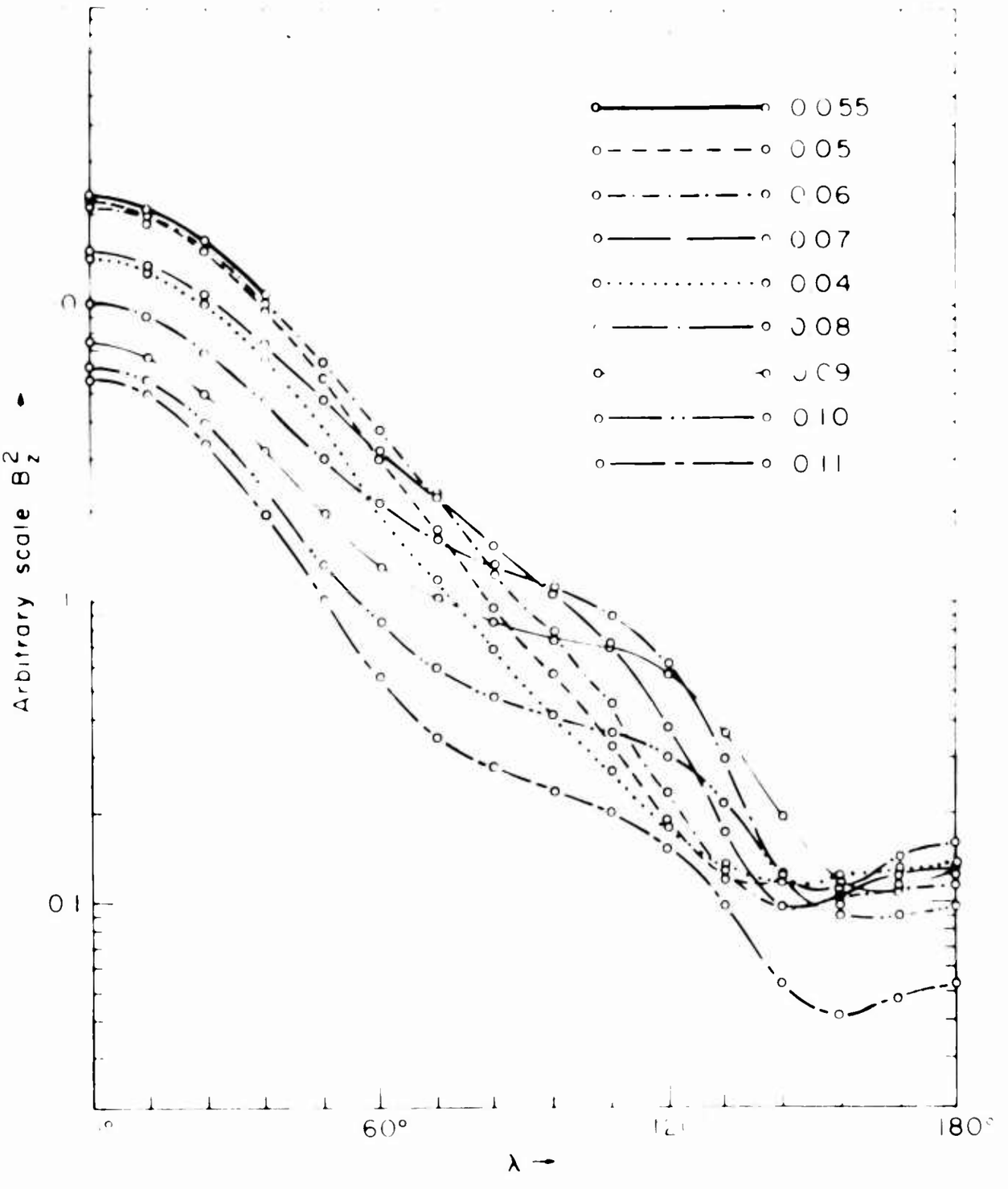

Figure 4 5-4 Plot of B_z^2 on surface vs λ

Plotted for several values of frequency

SUBSOLAR SOURCE DISTRIBUTION

micropulsations are located near local noon, the results found with the subsolar source distributions are in agreement with the observed diurnal variation of the level of activity.

CHAPTER V

SUMMARY AND CONCLUSIONS

WITH SUGGESTIONS FOR FURTHER WORK

5.1 Summary and Conclusions

This thesis was concerned with the effect that horizontal variations in the wave propagation properties will have upon the characteristics of Pc 2,3 observed on the earth's surface and with the manner in which these characteristics depend upon the position of the observer. The observed signal is the result of the oscillation of one or more modes of the ionospheric cavity. The form of the signal depends upon the individual mode properties and upon the extent to which the different modes are excited.

Each mode of the real three-dimensional cavity has a dependence upon each of the three coordinates, radius, latitude, and longitude. The Pc 2,3 oscillations are a result of the modes which have the lowest order dependence upon radius. The latitude and the longitude dependence of the modes was studied separately from each other.

There is a distinct series of latitude dependent modes. There is a significant difference between the periods of the low order latitude dependent modes. For example, the period of lowest order mode for the daytime model is 17.5 sec while the periods of the third and fifth order modes are, respectively, 13.0 and 11.5 sec. The period of the lowest order mode is determined by the conditions at the equator.

The observed daytime Pc 2,3 has little or no dependence upon latitude. This indicates that it is the oscillations of a single mode

which is being observed. Only the lowest order mode has a period which is compatible with the observed daytime Pc 2,3 periods.

The latitude dependence of the amplitude of the lowest order mode is, however, not in agreement with the observed daytime Pc 2,3 amplitude variation. The evidence in the literature is far from conclusive, but there have been isolated reports which find the maximum Pc 2,3 amplitudes occur at 30° and 60° latitude. The lowest order latitude dependent mode has its maximum amplitude at the equator. This discrepancy may be due to incorrect conclusions made from the limited observations of the amplitude variations or to deficiencies in the model. It is possible that the amplitudes of Pc 2,3 are not greatest at mid-latitudes; further systematic observations of the amplitude are needed to settle this question.

On the other hand, there are two deficiencies in the latitude dependent model which may be causing the discrepancy. Because the solutions are symmetric about the magnetic axis, the responce amplitude must be zero at the poles; this may force the mode amplitudes which are given by the model to be unnaturally low at high latitudes. The second deficiency in the model is that the ionospheric parameters depend only upon altitude. In the real ionosphere the electron density and the ion-neutral collision frequencies decrease with latitude. If we introduce this type of latitude dependence into the model values for the ionospheric parameters, the amplitude at high latitudes will be increased in comparison to the equatorial amplitude.

The lowest order latitude dependent mode is the mode which is principley excited by either a low latitude source or by a source which

is in phase over a large range of latitudes. Compact sources located at high latitudes will excite the higher order latitude dependent modes.

There appears to be a series of longitude dependent modes which have large amplitude responces in the daytime hemisphere and very small amplitudes in the nighttime hemisphere. The period of these modes is approximately the same as the resonant period given by a one-dimensional model for daytime conditions. Several of the longitude dependent modes have similar periods. Therefore, a source in the daytime hemisphere will excite several of these modes. Because of this very strong mode mixing, individual mode shapes cannot be determined by the technique we have employed.

Since these modes have small amplitudes in the nighttime hemisphere, the model predicts that a daytime source will not cause Pc 2,3 to be observed in the nighttime. It is probable that the sources and Pc 2,3 micropulsations are located in the daytime. If this is the case, then the prediction of the model is in good agreement with the low level of Pc 2,3 activity that is observed at night.

There also appears to be a series of longitude dependent modes which have large amplitudes in the nighttime hemisphere and very small amplitudes in the daytime hemisphere. The periods of these modes are approximately the same as the period predicted by a one-dimensional model for nighttime conditions. A source placed in the nighttime hemisphere of the longitude dependent model gives periods which agree with the observed nighttime periods. The transition from daytime to nighttime period in the model occurred as a smooth transition; this agrees with the smooth way in which the Pc 2,3 period is observed to

change as a function of local time.

In addition to these principle results concerning the mode structure, it was shown that the air layer has an important effect upon the field which is observed at the earth's surface. We demonstrated, for the case of isotropic conductivity, that the component of the magnetic field which is perpendicular to the direction of propagation will be small. In addition, it was shown that the presence of the air layer will decrease the Q's of the spectral peaks.

5.2 Suggestions for Further Work

Further observational data on Pc 2,3 is needed to determine the structure of the modes which are responsible for the observed Pc 2,3 oscillations. A phase change of 180^{o} occurs across the nodal lines of a mode. Therefore, since the amplitude distribution may be distorted by localized ionospheric damping, observing the relative phase at stations distributed over the earth's surface may be the best means for inferring the mode structure. We do not, however, wish to discourage a systematic study of the amplitude variation as a function of latitude and local time.

A study should be made to compare the variation of period with the changes in the state of the ionosphere. The results of chapter III show that the correlation should be greater if the equatorial electron density values are considered rather than mid-latitude electron density values.

The present study was limited to two-dimensional models. Additional information could be obtained with the use of three-dimensional models. An important feature which can be included in a three-

dimensional model, but not in two-dimensional models, is a point source, rather than the line source of two-dimensional models. The use of a point source would give a somewhat more realistic picture of the manner in which the responce amplitude varies with position than could be obtained with the two-dimensional models. However, the amount of computation necessary to solve a three-dimensional model numerically is quite large and it is not obvious that the additional results would justify the effort.

Perhaps a good idea of the way the cavity would be excited by a point source could be obtained by studying three-dimensional models in which the variation in one of the dimensions has been transformed out. If this procedure is employed, we may not use a completely arbitrary model. The properties of the model are not allowed to vary in the dimension which is transformed out. The solution of this model would require several solutions of a pair of coupled two-dimensional partial differential equations. This procedure would, however, require less computation than the computation that would be required to solve the full three-dimensional problem.

Although several studies have been made of the layered media problem for the cases in which propagation is in the north-south-vertical plane, we feel that there is still much to be learned from a layered problem for which the angle of propagation is arbitrary. There are two possible areas of investigation. First, there is the question of coupling between the fast and guided wave types which can be given more thorough consideration than we gave it in section 2.3. The second area is the very interesting question of the polariz-

ation of the surface field. The air layer will play an important role in determining the surface field. If the layered model results show that the transverse component of the magnetic field is eliminated when anisotropic, ionospheric conductivity is considered as it was eliminated for the isotropic conductivity studied in appendix I, we will then have a method for obtaining the direction of the wave propagation from the polarization of the surface fields.

The algebra involved in solving the layered problem for an arbitrary direction of propagation is very extensive when the layer matrices are obtained in the usual manner. The problem of obtaining these matrices is, however quite tractable when the matrizant method is employed (see Madden and Thompson [1964]).

APPENDIX I

Effect of the Air Layer, Located below the Ionosphere, on Micropulsations

In this appendix we will investigate the effect that the slightly ionized air layer, located between the surface of the earth and approximately 100 km altitude, has on incoming waves of micropulsation frequencies. In this layer the displacement current predominates over the conduction current. It will be shown that although at Pc 3 frequencies wave lengths in the neutral atmosphere are very long compared to the thickness of the air layer, this layer has an important effect on the magnetic field observed at the earth's surface.

The present discussions will be simplified by treating the conduction in the ionosphere as isotropic. Although the conductivity in the ionosphere is anisotropic, the following discussion is useful in pointing out an important difference between the behavior of TE waves (electric field transverse to the plane of propagation and TM waves (magnetic field transverse to the plane of propagation). In the models of chapters III and IV the propagation appears isotropic so the discussion in the appendix is applicable to these models.

Figure I-1 shows the geometry of the model. Let the plane of propagation be the x, z plane, where z is the upward vertical direction. The neutral atmosphere is represented by a layer $0 \leq z \leq h$ in which the propagation constant is $k_a = \omega/(\text{speed of light})$. The surface of the earth is represented by a perfect conductor at $z = 0$. In the atmosphere the space dependence of the waves is $e^{i(\ell x \pm n_a z)}$; the plus and minus signs indi-

FIG. I-1
GEOMETRY FOR
INVESTIGATION OF
AIR LAYER EFFECT

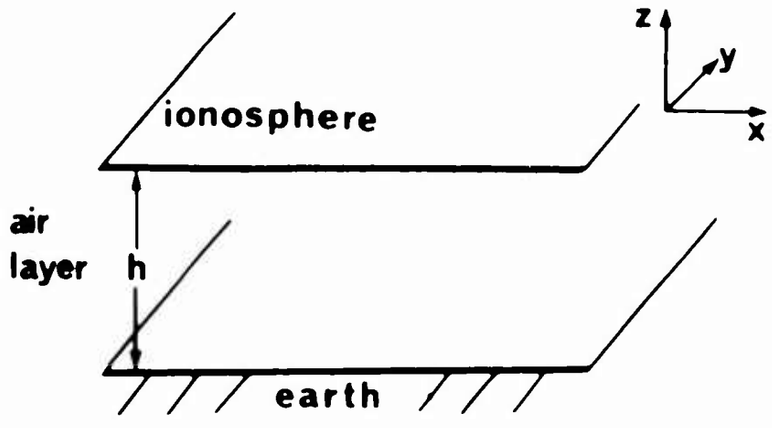

cate respectively upward and downward traveling waves. The dispersion relation is

$$k_a^2 = \ell^2 + n_a^2 \qquad \text{I.1}$$

The ionosphere is represented by a semi-infinite media in the region $z \geq h$. Let k_i be the isotropic propagation constant in the ionosphere. For the fast wave type, at .1 cps, the value of $|k_i|$ in the lower ionosphere takes values ranging from $(30\ \text{km})^{-1}$ to $(500\ \text{km})^{-1}$. In the ionosphere the space dependence of the waves is $e^{i[\ell x \pm n_i(z-h)]}$ and the dispersion relation is

$$k_i^2 = \ell^2 + n_i^2 \qquad \text{I.2}$$

The horizontal wave number ℓ must be the same in both media for the horizontal components of $\vec{E}$ and $\vec{H}$ to be continuous across the plane $z = h$. For disturbances with the horizontal extent observed for Pc 3 the value of $1/\ell$ will be on the order of a few thousand km.

Case of TE Propagation

In the TE the electric field has only a component in the y direction and the magnetic field is in the x,z plane. The matrix form for plane wave solutions obeying Maxwell's equation in the atmosphere is

$$V_a(z) = T_a(z) \begin{bmatrix} A_a \\ B_a \end{bmatrix}$$

where

$$T_a(z) = \begin{pmatrix} e^{in_a z} & e^{-in_a z} \\ -\frac{n_a}{\mu\omega} e^{in_a z} & \frac{n_a}{\mu\omega} e^{-in_a z} \end{pmatrix}$$

and

$$V_a(z) = \begin{pmatrix} E_y^a(z) \\ H_x^a(z) \end{pmatrix}$$

is the solution vector for the horizontal field components.

A_a and B_a are respectively the amplitudes of the outgoing and incoming waves in the air layer. Let the matrix C be defined as $C = T_a^{-1}(0)\, T_a^{-1}(h)$. The fields at the bottom of the atmospheric layer can be written in terms of the fields at the top as

$$V_a(0) = C\, V_a(h) \qquad \text{I.3}$$

For $1/\ell$ on the order of a few thousand km equation I.1 gives

$$n_a h \cong i\, \ell\, h \qquad \text{I.4}$$

Since $|n_a h| \ll 1$, $\sin(n_a h)$ and $\cos(n_a h)$ may be approximated by the first term of their Taylor expansions. C is then approximated by

$$C \cong \begin{pmatrix} 1 & i\mu\omega h \\ \dfrac{in_a^2 h}{\mu\omega} & 1 \end{pmatrix} \qquad \text{I.5}$$

In the ionosphere for a unit amplitude incoming wave

$$V_i(z) = T_i(z) \begin{pmatrix} A_i \\ 1 \end{pmatrix}$$

where

$$T_i(z) = \begin{pmatrix} e^{\delta} & e^{-\delta} \\ -\frac{n_i}{\mu\omega} e^{\delta} & \frac{n_i}{\mu\omega} e^{-\delta} \end{pmatrix} \qquad \text{I.6}$$

in which $\delta = i\, n_i(z-h)$. $V_i(z)$ is the solution vector for the ionosphere. Let S be the matrix $T_i(z)$ evaluated at $z = h$, at which point $e^{\pm\delta} = 1$. Define the matrix $D = C\,S$. Noting that some of the elements of C and S are 1, D is written

$$D = \begin{pmatrix} 1 + C_{12}S_{21} & 1 + C_{12}S_{22} \\ C_{21} + S_{21} & C_{21} + S_{22} \end{pmatrix} \qquad \text{I.7}$$

Since E_y and H_x are continuous across the plane $z = h$

$$V_a(h) = V_i(h) = S \begin{pmatrix} A_i \\ 1 \end{pmatrix} \qquad \text{I.8}$$

Using this equation and I.3 gives

$$V_a(0) = CV_a(h) = CS\begin{pmatrix} A_i \\ 1 \end{pmatrix} = D \begin{pmatrix} A_i \\ 1 \end{pmatrix} \qquad \text{I.9}$$

Since $E_y^a(0)$ must be zero, equation I.9 can be solved for A_i and $H_x^a(0)$. Again using $|\ell h| \ll 1$ we neglect $|\ell h|^2$ compared to unity. For values of $1/\ell$ of a few thousand kilometers $|\ell| \ll |k_i|$. Using this in equation I.2 gives $n_i^2 \cong k_i^2$. This approximation indicates the waves in the ionosphere are propagating in a near vertical direction. Solving I.9 with these approximations

$$A_i \cong -\frac{1 + ihk_i}{1 - ihk_i}$$

$$H_x^a(0) \cong \frac{2k_i}{\mu\omega}\left(\frac{1}{1 - ik_i h}\right) \qquad \text{I.10}$$

Putting this value of A_i into I.6 the horizontal electric field at the bottom of the ionosphere is

$$E_y^i(h) \cong A_i + 1 = \frac{-ihk_i}{1-ihk_i} \qquad \text{I.11}$$

If $|k_i h| \ll 1$ these results show that the electric field is small at the bottom of the ionosphere and that the surface magnetic field has twice the value of the field of the incoming wave. For the limit $h = 0$ these are the results normally obtained when an incoming wave is reflected by a perfect conductor. If $|k_i h|$ is on the order of unity, the magnetic field strength is not greatly changed, but the electric field at the bottom of the ionosphere does not vanish as it would if the air layer were absent. This behavior of the electric field may explain one of the results of the layered model study of Li et al. (1964). The waves studied in this work were predominantly TE. Several different angles of incidence in the north-south vertical plane were considered. For each the calculations were carried out with an air layer included and also with this layer removed. With the air layer included the Q of the resonant peaks were $\cong 2$. When the air layer was removed, the Q's went up to values of 3.5 to 4. The lower Q's in the case run with an air layer indicate more dissipation of

energy than in the cases when the air layer was absent. This extra dissipation may have been due to a higher electric field strength in the lower ionosphere.

Case of TM Propagation

The same type of matrix method used to study the TE case will be used to study the TM case. Some definitions will be changed as indicated. For the TM mode V_a, V_i, and T_a are defined as

$$V_a(z) = \begin{pmatrix} E_x^a(z) \\ H_y^a(z) \end{pmatrix} \qquad V_i(z) = \begin{pmatrix} E_x^i(z) \\ H_y^a(z) \end{pmatrix} \qquad \text{I.12}$$

$$T_a(z) = \begin{pmatrix} \frac{\mu\omega}{k_a^2} n_a e^{in_a z} & -\frac{\mu\omega}{k_a^2} n_a e^{-i\mu_a z} \\ e^{in_a z} & e^{-n_a z} \end{pmatrix}$$

The assumption is made that $k_a \ll \ell$, then from I.1 $n_a \approx i\ell$. The matrix C is given by

$$C \cong \begin{pmatrix} 1 & \frac{i\mu\omega}{k_a^2}\ell^2 h \\ -\frac{ik_a^2}{\mu\omega} h & 1 \end{pmatrix}$$

For TM propagation the matrix S is given by

$$S = \begin{pmatrix} \frac{\mu\omega n_i}{k_i^2} & -\frac{\mu\omega n_i}{k_i^2} \\ 1 & 1 \end{pmatrix} \qquad \text{I.13}$$

From I.2, if $|k_i| \gg \ell$, the approximation may again be made that $n_i \cong k_i$. The matrix D is given by

$$D \cong \begin{pmatrix} S_{11} + C_{12} & S_{12} + C_{12} \\ C_{21}S_{11} + 1 & C_{21}S_{12} + 1 \end{pmatrix}$$

Equation I.9 is solved for A_i and $H_y^a(0)$ again using the fact that the electric field disappears at z = 0.

$$A^i = \frac{1 - R}{1 + R} \qquad \text{I.14}$$

$$H_y^a(0) = 2/(1 + R) \qquad \text{I.15}$$

where

$$R = i\, k_i\, h\, \frac{\ell^2}{k_a^2}$$

The value of $\left|\frac{\ell^2}{k_i}\right|$ is roughly 10^5 to 10^6 so $R \gg 1$. Then

$$A_i \cong -1$$

$$H_y^a(0) \cong 2/R \qquad \text{I.16}$$

Putting this value of A_i together with S as given by I.13 into I.8 gives

$$E_x^i(h) = \frac{\mu\omega}{k_i}(A_i - 1) \simeq \frac{-2\mu\omega}{k_i} \qquad 1.17$$

Equation I.17 shows that the electric field strength at the base of the ionosphere is twice that of the electric field of the incoming wave. This is in contrast with the zero value in the case when no atmospheric layer is involved in the model.

Equation I.15 shows that if no atmospheric layer were present, the surface magnetic field would be 2. Equation I.16 shows, in contrast, that the transverse component of the surface magnetic field is decreased by the large factor R due to the presence of the atmospheric layer. This large effect of the air layer, despite its small thickness relative to the wave lengths involved, is due to the very great difference between k_a and k_i.

Nishida (1964) considered the screening effect, of the ionosphere and neutral atmosphere, on waves propagating in the north-south direction. Incoming waves of both the fast and guided type were considered. With the incoming fast waves the magnetic field is in the plane of propagation and the waves are therefore TE. The incoming guided waves, on the other hand, are TM but through Hall conductivity coupling a small north-south component of the magnetic field is introduced. Nishida showed that, when the propagation was in the north-south-vertical plane, the magnetic field observed on the surface would be almost purely north-south, for either type of incoming wave. The present author suggests that this

behavior is a result of the destruction of the component of the magnetic field transverse to the direction of propagation.

APPENDIX II

Solution of Chapter III Model by Means of Difference Equations

Difference Equation Grid

A finite difference method was used to solve equation 3.2.5. A grid was set up which covered the portion of the r,x plane for $r_e \leq r \leq r_m$, $0 \leq x \leq 1$. This region has already been shown in figure 3.3-2.

The vertical grid lines at x = .0, .08, .16, .24, .34, .44, .54, .64, .76, .88, and 1.0. The horizontal grid lines are at the altitudes for which ionospheric parameter values are given in Table 2.1-1 and Table 2.1-2.

There are 11 grid lines between the equator and the pole. Therefore, the distance between the vertical grid lines is approximately $(\frac{1}{10} \frac{\pi}{2} r_e) \approx$ 1000 km. Now, in the lower ionosphere the spacings between the horizontal grid lines is as little as 30 km. Therefore, it is necessary to determine if the unequal spacing of the grid lines will introduce significant errors into the resonant frequencies which will be determined using the difference equations. This question is considered in appendix VI. The results of this appendix show that the uneven grid spacing which was used will give results which are accurate to better than 5 per cent for modes up to n = 5.

The strength of the source g in equation 3.2.5 is constant in each of the blocks described by $r_i \leq r \leq r_{i+1}$, $x_j \leq x \leq x_{j+1}$. The value of g in these blocks is denoted by $g_{i,j}$.

Presentation of the Difference Equations at the Gridpoints

We now present the derivation of the difference equation which approximates the partial differential equation, equation 3.2.5; the difference equation formed at each grid point, is a linear equation. For convenience, equation 3.2.5 is written again:

$$\frac{1}{r^2}\frac{\partial^2 \Psi}{\partial x^2} + \frac{1}{1-x^2}\frac{\partial^2 \Psi}{\partial r^2} + \frac{k_f^2 \Psi}{1-x^2} = \frac{g}{1-x^2} \qquad \text{II.1}$$

Forsythe and Wasow (1960, p. 160) show that we may find the solution to this partial differential equation which satisfies the boundary conditions of section 3.4 by making the variation of a certain integral, J, disappear. J is given by

$$J = \iint_{\text{region}} \left[\frac{1}{2r^2}\frac{\partial^2 \Psi}{\partial x^2} + \frac{1}{2(1-x^2)}\frac{\partial^2 \Psi}{2r^2} - \frac{k_f}{2(1-x^2)}\Psi^2 + \frac{g\Psi}{1-x^2} \right] dx\, dr$$

$$+ \oint_{\text{boundary}} \frac{1}{2} a_1 \Psi^2 \, ds$$

The boundary conditions of section 3.4 are all homogeneous and of the form

$$a_1 \Psi + a_2 \Psi_N = 0$$

where ψ_n is the derivation of ψ in the direction normal to the boundary. It is only on boundary B4 that $a_1\psi_1$ is nonzero; therefore, the only contribution to the boundary integral is from this boundary. On boundary B4 (see Forsythe and Wasow [1960, p. 161]).

$$a_2 = \frac{1}{1-x^2}$$

Therefore

$$a_1 = \left(\frac{1}{1-x^2}\right) \left(\frac{1}{r} + ik_f \cos \bar{\alpha}\right)$$

We will obtain the difference equation at point 1 of figure II-1. A subscript ℓ on ψ or k_f indicates that the quantity is evaluated at the ℓ-th gridpoint. The source strength, $g_{i,j}$, is constant over the block in which $g_{i,j}$ appears in figure II-1. The same is true for $g_{i,j+1}$, $g_{i+1,j}$ and $g_{i+1,j+1}$.

Applying the condition that the variation of J vanish gives the difference equation, for point 1, as

$$\psi_1 \left\{ \frac{1}{2r_1} (a+b) \left(\frac{1}{c} + \frac{1}{d}\right) + \frac{1}{2(1-x_1^2)} (c+d) \left(\frac{1}{a} + \frac{1}{b}\right) \right.$$

$$\left. - \frac{k_{f_1}^2}{4(1-x_1^2)} (a+b)(c+d) \right\} \qquad \leftarrow \left(\begin{array}{l} \text{We will} \\ \text{refer to} \\ \text{this term} \\ \text{as Term 2.} \end{array} \right)$$

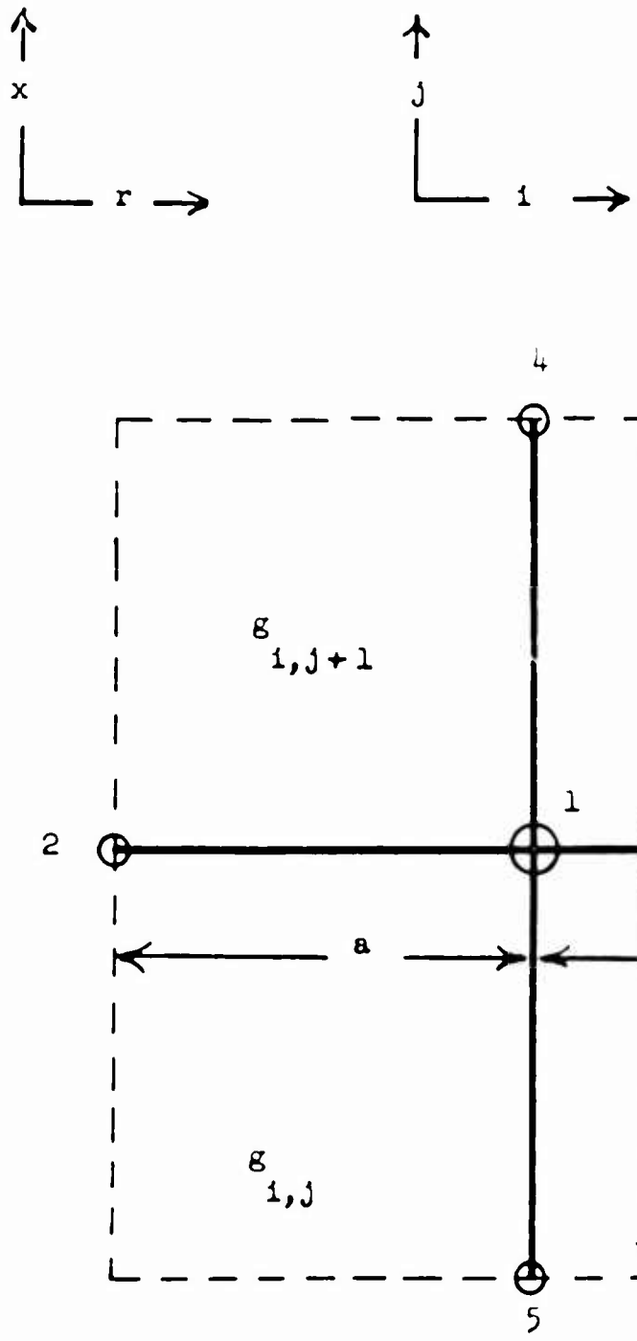

Figure II-1

Geometry for Deriving Difference Equation

$$- \psi_4 \left\{ \frac{1}{2r_1^2} \left(\frac{a+b}{c}\right) \right\}$$

$$- \psi_5 \left\{ \frac{1}{2r_1^2} \left(\frac{a+b}{d}\right) \right\}$$

$$- \psi_3 \left\{ \frac{1}{2(1-x_1^2)} \left(\frac{c+d}{b}\right) \right\}$$

$$- \psi_2 \left\{ \frac{1}{2(1-x_1^2)} \left(\frac{c+d}{a}\right) \right\}$$

$$+ \frac{1}{4(1-x_1^2)} \left\{ ac\ g_{i,j+1} + ad\ g_{i,j} + bd\ g_{i+1,j} + bc\ g_{i+1,j+1} \right\} = 0 \qquad \text{IL2}$$

For the grid points at 100 km, which are on the boundary between the ionosphere and the air layer, term 2 is modified to

$$- \frac{1}{r(1-x_1^2)} \left[k_a^2\, a(c+d) + k_{f_1}\, b(c+d) \right]$$

where k_a is the free space propagation constant.

For a point on the outer boundary of the region, B4, the condition of outward propagation waves leads to the difference equation

$$\psi_1 \left\{ \frac{1}{2r_1^2}\, a \left(\frac{1}{c} + \frac{1}{d}\right) + \frac{1}{2(1-x_1^2)} (c+d)\, \frac{1}{a} \right.$$

$$\left. - \frac{k_{f_1}^2}{4(1-x_1^2)}\, a\,(c+d) - \frac{1}{2(1-x_1^2)} \left(\frac{1}{r} + ik_{f_1} \cos \bar{\alpha}\right) (c+d) \right\}$$

$$- \psi_4 \left\{ \frac{1}{2r_1^2} \quad \frac{a}{c} \right\}$$

$$- \psi_5 \left\{ \frac{1}{2r_1^2} \quad \frac{a}{d} \right\}$$

$$- \psi_2 \left\{ \frac{1}{2(1-x_1^2)} \left(\frac{c+d}{a}\right) \right\} = 0$$

Solution of the Set of Linear Difference Equations

The set of difference equations is a set of linear equations for the unknowns $\psi_{i,j}$. These difference equations are of the elliptic type; much of the literature concerning the solution of elliptic difference equations considers the use of relaxation methods for solving large size sets of such equations. An attempt was made to compute a solution to the present set of difference equations with a relaxation method. It was found that the relaxation method did not converge to a solution. To help us understand why the relaxation did not converge, an analysis was made of the application of a relaxation method to the scalar wave equation. The scalar wave equation is similar in character to equation II.1. The analysis is given in appendix V. The results of this appendix added to our computational experience indicate that relaxation methods are not suitable to wave like equations.

After it was found that relaxation methods were not suitable, a direct method was developed to solve the set of linear equations. This method

is presented in appendix IV. The amount of computation and computer storage used in the application of this method is less than that required for the direct methods available in the literature.

Source Distributions Which Were Used to Excite Individual Modes

To examine the mode structure and resonant frequency of individual modes, source distributions were used which excited one mode to a much greater degree than any other mode. The now zero values of the source terms $g_{i,j}$ are given in Table II-1. D1 denotes the daytime n = 1 sources, N1 the nighttime n = 1 sources, etc.

TABLE II-1

Sources Used to Excite Individual Modes

Nonzero Values of $g_{i,j}$

	For the Daytime Sources i = 17			For the Nighttime Sources i = 8		
J	D1	D3	D5	N1	N3	N5
2	9.	3.	10.	9.	3.	5.
3	7.	1.	0.	7.	1.	3.
4	5.	-1.	-10.	5.	-1.	-3.
5	3.	-2.	-5.	3.	-2.	-5.
6	1.	-3.	1.	1.	-3.	-3.
7	.5	-2.	10.	.5	-2.	-1.
8	.3	-1.	5.	.3	-1.	1.
9	.1	-.5	2.	.1	-.5	1.

Localized Source Distributions

The low latitude (0.° to 9.° latitude) source distribution was

$$g_{17,2} = 1.$$

$$g_{17,3} = .5$$

$$g_{17,4} = .2$$

The higher latitude (39.5° to 49.0° latitude) source distribution was

$$g_{17,9} = 1.$$

APPENDIX III

Solution of Chapter IV Model by Means of Difference Equations

Difference Equation Grid

A finite difference method was used to solve equation 4.1.10. A grid was set up which covered the region of the r, λ pland for $r_e \leq r \leq r_m$, $0^\circ \leq \lambda \leq 180^\circ$. This region has already been shown in figure 4.1-1.

The vertical grid lines are located at $\lambda = 0.^\circ, 12.^\circ, 24.^\circ, \ldots, 180.^\circ$. The horizontal grid lines are at the altitudes for which ionospheric parameter values are given in Table 2.1-1 and Table 2.1-2.

Presentation of the Difference Equations at the Gridpoints

We now present the difference equation which was used to approximate the partial differential equation, equation 4.1.10. For convenience this equation is written again:

$$\frac{\partial}{\partial r}\left(\frac{r}{\sigma}\frac{\partial H}{\partial r}\right) \qquad \text{(term 1)}$$

$$+\frac{\partial}{\partial \lambda}\left(\frac{1}{r\sigma}\frac{\partial H}{\sigma \lambda}\right) \qquad \text{(term 2)}$$

$$+ \cdot \mu \omega r H - S = 0 \qquad \text{(term 3)} \quad \text{III.1}$$

The subscripts e and z which were used in chapter IV have been dropped from H_z and σ_e. The grid used in deriving the difference equations is shown in figure III-1. The difference equation is derived for the center

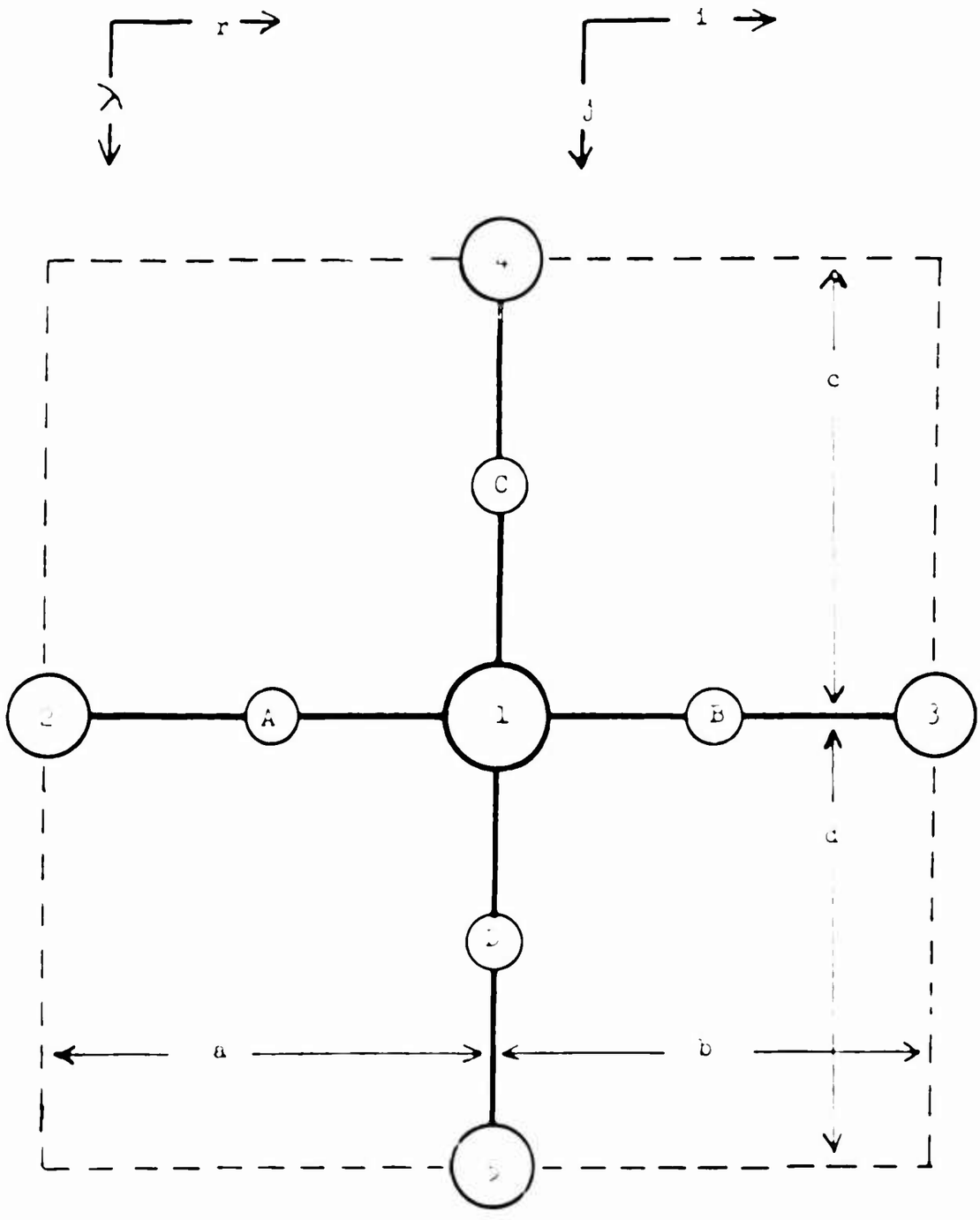

Figure III-1

Geometry for Deriving Difference Equation

point, denoted as 1. The spacing in the r direction between points 1 and 2 is a; the point half way between points 1 and 2 is denoted by A. Analogous notation is used for the other grid lines. The symbol $|_A$ means: evaluated at A. The notation H_1 means: H evaluated at point 1. Analogous notation is used for the other points.

The finite difference representation for term 1 of equation III.1 is given by

$$\left[\frac{r}{\sigma}\Big|_B \frac{\partial H}{\partial r}\Big|_B - \frac{r}{\sigma}\Big|_A \frac{\partial H}{\partial r}\Big|_A \right] \Big/ \frac{1}{2}(a+b)$$

where

$$\frac{\partial H}{\partial r}\Big|_B = (H_3 - H_1)/b$$

and

$$\frac{\partial H}{\partial r}\Big|_A = \left[H_1 - H_2 \right] / a$$

Similarly, the representation for term 2 is given by

$$\left[\frac{\sigma}{r}\Big|_D \frac{H_5 - H_1}{d} - \frac{\sigma}{r}\Big|_C \frac{H_1 - H_4}{c} \right] \Big/ \frac{1}{2}(c+d)$$

The representation for term 3 is

$$i\mu\omega H_1 - S_1$$

We now give the difference equation for the case when point 1 is a point on the boundary B4 of figure 4.1-1. The condition on this boundary was discussed in section 4.2.

Term 2 of equation III.1 is 0, because the boundary condition on boundary B4 is that waves are propagating radially outward at points on this boundary. The value of H_3 is approximately,

$$H_3 \cong H_2 + \left.\frac{\partial H}{\partial r}\right|_1 (a+b) \qquad \text{III.2}$$

Equation 4.2.1 gives

$$\left.\frac{\partial H}{\partial r}\right|_1 = ik_f H_1$$

Putting this expression into equation III.2 enables us to eliminate H_3 from the finite difference representation for term 1 of equation III.1.

Solution of the Set of Linear Difference Equations

A difference equation was written for each gridpoint of the region. These difference equations are a set of linear equations. The algorithm used to solve the set of equations is given in appendix IV.

APPENDIX IV

Matrix Method for the Solution of Difference Equations

The set of difference equations for a M x N grid form a set of M x N linear equations. If the equations at grid points (i,j) are arranged in the order

$$(1,1),\ (1,2),\ \cdots,\ (1,N)$$

$$(2,1),\ (2,2),\ \cdots,\ (2,N)$$

$$\vdots$$

$$(M,1),\ (M,2),\ \cdots,\ (M,N)$$

then, since each grid point is connected only to its neighbors, the set of equations is of the form

$$TV = S$$

where T is the coefficient matrix which may be written in the partitioned form

$$T = \begin{bmatrix} A_1 & C_1 & 0 & \cdots & 0 \\ D_1 & A_2 & C_2 & & \vdots \\ 0 & D_2 & A_3 & & \vdots \\ \vdots & & \ddots & & 0 \\ \vdots & & & & C_{M-1} \\ 0 & \cdots & 0 & D_{M-1} & A_M \end{bmatrix}$$

A_k, C_k, and D_k are N x N square matrices. Moreover, C_k and D_k are diagonal matrices. We partition V and S in the following manner

$$V = \begin{bmatrix} V_1 \\ V_2 \\ \vdots \\ V_M \end{bmatrix} \qquad S = \begin{bmatrix} S_1 \\ S_2 \\ \vdots \\ S_M \end{bmatrix}$$

Here V_k and S_k are column vectors of length N.

Because of the form of T, a very convenient direct method of solving for V consists of partitioning T into two triangular matrices

$$T = E\,F$$

$$E = \begin{bmatrix} I & 0 & \cdots & 0 \\ E_1 & I & & \vdots \\ 0 & E_2 & I & \\ \vdots & \ddots & \ddots & \\ 0 & \cdots & 0 & E_{M-1} \quad I \end{bmatrix}, \quad F = \begin{bmatrix} F_1 & G_1 & 0 & \cdots & 0 \\ 0 & F_2 & G_2 & & \vdots \\ \vdots & \ddots & \ddots & \ddots & \\ & & & & G_{M-1} \\ 0 & \cdots & & 0 & F_M \end{bmatrix}$$

To obtain the elements of E and F, start by post multiplying F by E and equating the product to T.

$$EF = \begin{bmatrix} F_1 & & & & & 0 \\ E_1F_1 & F_2+E_1G_1 & G_2 & & & \cdot \\ 0 & E_2F_2 & F_3+E_2G_2 & & & \cdot \\ \cdot & \cdot & \cdot & & & \cdot \\ \cdot & & & \cdot & & \\ \cdot & & \cdot & & \cdots & 0 \\ 0 & \cdot & \cdot & \cdot & 0 \; E_{M-1}F_{M-1} & F_M+E_{M-1}G_{M-1} \end{bmatrix}$$

Then proceed in the following order to obtain the elements of E and F.

$$F_1 = A_1$$
$$E_1 = D_1F_1^{-1}$$
$$F_2 = A_2-E_1G_1$$
$$\vdots$$
$$E_k = D_kF_k^{-1}$$
$$F_{k+1} = A_{k+1}-E_kG_k$$
$$\vdots$$
$$F_M = A_M-E_{M-1}\,G_{M-1}$$

Having obtained E and F we may easily solve for V. Define an intermediate vector Z

$$Z = FV$$

$$Z = \begin{bmatrix} Z_1 \\ Z_2 \\ \cdot \\ \cdot \\ \cdot \\ Z_M \end{bmatrix}$$

The Z_k are column vectors of length N. Then

$$EZ = S$$

$$Z_1 = S_1$$
$$Z_k = S_k - E_{k-1} Z_{k-1} \qquad k = 2, \cdots, M$$

Finally we obtain the solution V.

$$V_M = Z_{M-1}$$

$$V_k = F_k (Z_k - G_k V_{k+1}) \qquad k = M-1, M-2, \ldots, 1$$

Note that the F_k^{-1} matrices were computed in the process of getting the E matrix.

The operations which require the main bulk of the computation are the matrix multiplication $D_k F_k^{-1}$ and the inversion of the matrix F_k. Both of these operations increase as N^3, and have to be done M times.

Therefore the total number of operations increases as MN^3. The ordinary direct methods of solving linear equations go as the number of equations to the third power or $(MN)^3$. The present method is convenient if one wishes to obtain solutions for several different source vectors S. First the E_k and F_k^{-1} matrices are obtained. Then each solution requires only multiplications of vectors by matrices.

If, on the other hand, computer storage is at a premium, then the Z_k vectors may be found as the E_k and F_k matrices are computed. It will then only be necessary to retain the F_k^{-1} and not the E_k matrices.

To assure that round-off errors did not seriously affect the solution consider a residual vector R given by

$$R = TV - S$$

or in component form

$$r_i = \sum_{j=1}^{MN} T_{ij}\, v_j - s_i \qquad i = 1,2,\cdots,MN$$

R would, of course, be a null vector, if no round-off errors were present. Examination of R in the computations carried out in this thesis showed that

$$|r_i| \leq 10^{-7} \sum_j |T_{ij}\ v_j|$$

which indicates round-off error was not important.

APPENDIX V

Divergence of Relaxation Method

In general practice, the solution of elliptic difference equations, such as Laplace's equation, is obtained by the use of relaxation methods. It is tempting to use these rapid, easily programed methods for the solution of equations governing wave propagation. Unfortunately, they fail to converge to a solution when applied to such problems. In the present investigation relaxation methods were applied initially. These methods were abandoned, however, when the computations failed to converge to a solution.

In this appendix we show that a basic relaxation technique, known as the point Jacobi method (also called "simultaneous displacement") diverges if applied to the reduced wave equation in a rectangular region when the frequency is above the lowest resonance frequency of the region. In arriving at this proof a method of analysis is used which is similar to the method used to obtain the convergence rate for relaxation solutions to Laplace's equation. (See Young [1962] p. 405.)

The region will be taken as the rectangle $0 \leq r \leq L_r$, $0 \leq y \leq L_y$. Let h and d respectively be the spacing in the r and y directions. The number of grid points in the r and y directions then are

$$M = \frac{L_r}{h} + 1$$

$$N = \frac{L_y}{d} + 1$$

Let $Q=(M-1)(N-1)$. Let the boundary condition be that the unknown, V, be 0 on the boundaries. The difference equation approximation to the reduced

wave equation is

$$\frac{V_{i+1,j}-2V_{i,j}+V_{i-1,j}}{h^2} + \frac{V_{i,j+1}-2V_{i,j}+V_{i,j-1}}{d^2} + k^2 V_{i,j} = S_{i,j}$$

$$i = 1,\cdots,M-1 \qquad j = 1,\cdots,N-1 \qquad \text{V.1}$$

Where $S_{i,j}$ are source terms.

The Jacobi method develops the $\ell+1$-th iteration from the ℓ-th iteration by solving for $V^{\ell+1}_{i,j}$ in terms of the values at the neighboring grid point. The iteration is written

$$V^{\ell+1}_{i,j} = \beta\,[d^2(V^{\ell}_{i+1,j} + V^{\ell}_{i-1,j}) + h^2(V^{\ell}_{i,j+1} + V^{\ell}_{i,j-1})] - \beta S_{i,j} d^2 h^2 \qquad \text{V.2}$$

Where

$$B = \frac{1}{2\Delta - k^2 h^2 d^2}$$

$$\Delta = d^2 + h^2$$

It is now convenient to introduce matrix notation. Let V^{ℓ} be the vector of length Q, giving the ℓ-th iteration values and let $V^{\ell+1}$ be the vector after the next iteration. Let S be the source vector. Then, the connection between $V^{\ell+1}$ and V^{ℓ} may be written

$$V^{\ell+1} = \mathcal{L} V^{\ell} - (\beta d^2 h^2) S$$

$\mathcal{L}$ being the square Q x Q matrix whose elements are given by the equation V.2. Let the true solution be V_T and the error at the ℓ-th

step be V_e^l . Then

$$V^{l+1} = V_T + V_e^{l+1} = \mathcal{L} V_T + \mathcal{L} V_e^l - (\beta d^2 h^2) S .$$

But since $V_T = \mathcal{L} V_T - (\beta d^2 h^2) S$

$$V_e^{l+1} = \mathcal{L} V_e^l$$

Let the Q eigen vectors of $\mathcal{L}$ be $E_{m,n}$ and let the corresponding eigen values be $\lambda_{m,n}$. We may then expand V_e^l in terms of the $E_{m,n}$

$$V_e^l = \sum a_{m,n} E_{m,n}$$

and

$$V_e^{l+1} = \mathcal{L} \sum a_{m,n} E_{m,n} = \sum \lambda_{m,n} a_{m,n} E_{m,n}$$

For the iteration to converge to the true solution the magnitude of all $\lambda_{m,n}$ must be less than 1.

Each of the eigen vectors, $E_{m,n}$, has the components

$$\xi_{i,j} = \sin i \alpha_m \sin j \alpha_n$$

where

$$\alpha_m = \frac{\pi h}{L_r} m \qquad \alpha_n = \frac{\pi d}{L_y} n$$

To show this, begin by operating on the eigen vector with $\mathcal{L}$. This is equivalent to applying V.2 to each component of the eigen vector. The i,j component after the operation is

$$\lambda_{m,n} \sin i \alpha_m \sin j \alpha_n \qquad V.3$$

where

$$\lambda_{m,n} = \left\{2\beta \left[d^2 \cos \alpha_m + h^2 \cos \alpha_n\right]\right\} \qquad V.4$$

Note that $\lambda_{m,n}$ does not depend on i or j. This shows that $E_{m,n}$ is an eigen vector and $\lambda_{m,n}$ is the corresponding eigen value.

The propagation constant associated with the lowest resonant frequency is given by

$$k_1^2 = \left(\frac{\pi}{L_x}\right)^2 + \left(\frac{\pi}{L_y}\right)^2 \qquad V.5$$

Equation V.4 shows that the largest eigen value is λ_{11} (this is not strictly true since $\lambda_{m-1,n-1} = \lambda_{1,1}$). The reason λ_{11} is the largest eigen value is that the factor cos α_m, of equation V.4, has its largest value for m = 1 and the factor cos α_n has its largest value for n = 1. At frequencies near the lowest resonance dk, hk $\ll$ 1. If the cosine factors in $\lambda_{1,1}$ are expanded in Taylor series, and afterwards only terms up to the second order are retained,

$$\lambda_{1,1} = 1 + \frac{h^2 d^2}{2\Delta}\left[k^2 - \left(\frac{\pi}{L_x}\right)^2 - \left(\frac{\pi}{L_y}\right)^2\right] \qquad V.6$$

This equation shows that if $k > k_1$, then $\lambda_{1,1} > 1$ and therefore, the iteration V.2 will not converge to a solution of $k > k_1$. For this reason, the Jacobi relaxation method is suitable only for frequencies below the lowest resonance. Notice that this result is independent of the grid spacing.

APPENDIX VI

Evaluation of Error Due to Grid Spacing

In this appendix, we examine the size of the error in resonant frequency which results when a finite difference method is used to solve the scalar wave equation. The size of this error, for a one-dimensional region, has been considered by previous authors (see Madden and Thompson [1964] or Hildebrand [1952]). We will consider a two-dimensional region and, in particular, a region with dimensions typical of the ionospheric cavity. This cavity extends much further in the horizontal than in the vertical direction. Therefore if we have approximately the same number of grid points in both directions, the finite difference grid will have a larger spacing in the horizontal direction.

The region we consider is the rectangle in the y, r plane given by $0 \leq y \leq L_y$, $0 \leq r \leq L_r$. This region has been shown in figure 3.4-1. The unknown, V, obeys the same boundary conditions as it did in section 3.4, i.e., $V = 0$ on all boundaries except for the boundary line $r = L_r$. On this boundary $\frac{\partial V}{\partial r} = 0$. We impose a grid upon this region with the grid points given by

$$r_i = ih \qquad i = 0,1,\cdots,M$$

$$y_j = jd \qquad j = 0,1,\cdots,N$$

where d and h are respectively the horizontal and vertical spacing.

The difference approximation to the scalar wave 3.4.2 is

$$\frac{V_{i+1,j}-2V_{i,j}+V_{i-1,j}}{h^2}+\frac{V_{i,j+1}-2V_{i,j}+V_{i,j-1}}{d^2}+\hat{k}^2V_{i,j}=0 \qquad \text{VI.1}$$

In this equation $V_{i,j}$ is the value of V at the i,j-th grid point. In a manner analogous to the method of separation of variables which is used to solv the wave equation, the difference equation may be solved by writing

$$V_{i,j}=R_iY_j \qquad \text{VI.2}$$

where R_i depends only on i and Y_j only on j. These functions obey the difference equations

$$\left.\begin{aligned} R_{i+1}-2R_i+R_{i-1}+h^2\hat{k}_r^2R_i&=0\\ Y_{j+1}-2Y_j+Y_{j-1}+d^2\hat{k}_y^2Y_j&=0\end{aligned}\right\} \qquad \text{VI.3}$$

when

$$\hat{k}^2=\hat{k}_r^2+\hat{k}_y^2$$

The solutions to VI.3 which obey the boundary conditions are

$$\begin{cases} R_i = \sin \frac{i\pi}{2M} (2m-1) \\ Y_j = \sin \frac{j\pi}{N} \quad n \end{cases} \qquad \text{VI.4}$$

In order for the solutions in VI.4 to satisfy VI.3 $\hat{K}_r^2$ and $\hat{K}_y^2$ must have the values

$$\left.\begin{aligned} \hat{k}_r^2 &= \frac{4}{h^2} \sin^2 d_m \qquad m = 1,\cdots,M \\ \hat{k}_y^2 &= \frac{4}{d^2} \sin^2 \alpha_n \qquad n = 1,\cdots,N \end{aligned}\right\} \qquad \text{VI.5}$$

where

$$\alpha_m = \frac{\pi}{4m} (2m-1) \qquad \alpha_n = \frac{n\pi}{2N}$$

For the lower modes $n \ll N$ and $m \ll M$ so the $\sin^2 \left\{ \begin{matrix} \alpha_n \\ \alpha_m \end{matrix} \right\}$ factors may be expanded in Taylor series. Retaining only the two lowest order terms in α_n and α_m gives the approximations

$$\begin{aligned} k_r^2 &\cong \left[\frac{4}{h^2}\right] \left[\alpha_m^2\right] \left[1 - \frac{\alpha_m^2}{3}\right] \\ &= \left[\frac{\pi}{2L_r} (2m-1)\right]^2 \left[1 - \frac{\alpha_m^2}{3}\right] \\ k_y^2 &\cong \left[\frac{4}{d^2}\right] \left[\alpha_n^2\right] \left[1 - \frac{\alpha_n^2}{3}\right] \\ &= \left[\frac{\pi}{L_y} n\right]^2 \left[1 - \frac{\alpha_n^2}{3}\right] \end{aligned} \qquad \text{VI.6}$$

Let $\hat{f}_{m,n}$ be the resonant frequency given by the difference equations, and let v_a be the wave velocity.

$$\hat{f}^2_{m,n} = \left(\frac{v_a}{2\pi}\right)^2 \hat{k}^2$$

Using the expressions VI.6

$$\hat{f}^2_{m,n} \simeq \left(\frac{v_a}{2\pi}\right)^2 \left\{\left[\frac{\pi}{2L_r}\ (2m-1)\right]^2 \left[1 - \frac{\alpha_m^2}{3}\right] + \left[\frac{\pi n}{L_y}\right]^2 \left[1 - \frac{\alpha_n^2}{3}\right]\right\} \qquad \text{VI.7}$$

The exact resonant frequencies, $f_{m,n}$, for the wave equation were given in equation 3.4.4. Let the relative error, E_{rel}, in the resonant frequency, be defined as

$$E_{rel} = \frac{f_{m,n} - \hat{f}_{m,n}}{f_{m,n}} \qquad \text{VI.8}$$

Now for $E_{rel} \ll 1$

$$E_{rel} \simeq \frac{1}{2}\ \frac{f^2_{m,n} - \hat{f}^2_{m,n}}{f^2_{m,n}} \qquad \text{VI.9}$$

The value of $f^2_{m,n}$ in the denominator may be approximated by

$$f^2_{m,n} \simeq \left(\frac{v}{2\pi}\right)^2 \left[\frac{\pi}{2L_r}\ (2m-1)\right]^2 \qquad \text{VI.10}$$

Using this in equation VI.9 gives

$$E_{rel} \simeq \frac{1}{2}\ \frac{\alpha_m^2}{3} + \left\{ \frac{1}{2}\ \frac{\alpha_n^2}{3} \left(\frac{\pi n}{L_y} \right)^2 \Big/ \left[\frac{\pi}{2L_r}\ (2m-1) \right]^2 \right\}$$

$$= \frac{1}{6} \left[\frac{\pi}{4M}\ (2m-1) \right]^2 + \frac{1}{6} \left[\frac{\pi}{N}\ \frac{L_r}{L_y}\ \frac{n^2}{2m-1} \right]^2 \qquad \text{VI.11}$$

The first term of this expression depends on the grid spacing in the vertical direction, while the second term reflects the horizontal grid spacing.

Expression VI.11 was used to evaluate E_{rel} for several modes. In table VI-1 we give E_{rel}, for values similar to that used in the numerical solutions. These values used in the evaluation were

$M = 10$

$N = 20$

$L_r = 1{,}500$ km

$L_y = 15{,}000$ km

TABLE VI-1

Relative Error in Frequency

m	n	E_{rel}
1	1	.010
1	2	.011
1	3	.014
1	5	.036

The contribution of the first term to the values of E_{rel} was .010. From this we see that for $n \leq 3$ the major error results from the vertical spacing, while for $n = 5$ it results from the horizontal spacing.

BIBLIOGRAPHY

Benioff, H., Observations of geomagnetic fluctuations in the period range 0.3 to 120 seconds, J. Geophys. Res., 65, 1413-1422, 1960.

Bolshakova, O. V., and K. Y. Zubin, On the frequency of occurrence and amplitude spectrum of the geomagnetic field pulsations, Ann. Geophys., 17, 345-350, 1961.

Bostick, F. X., Jr., Propagation characteristics of plane, small amplitude hydromagnetic disturbances in the earth's upper atmosphere, Ph.D. thesis, University of Texas, Austin, 1964.

Bostick, F. X., Jr., and H. W. Smith, Investigations of large-scale inhomogeneities in the earth by the magneto-telluric method, Proc. IRE, 50, 2339-2346, 1962.

Campbell, W. H., Studies of magnetic field micropulsations with periods of 5 to 30 seconds, J. Geophys. Res., 64, 1819-1826, 1959.

Chapman, S., The electrical conductivity of the ionosphere; a review, Nuovo Cimento, 4, Suppl., 1385-1412, 1956.

Courant, R., and D. Hilbert, Methods of Mathematical Physics, Vol. II, Interscience Publishers, New York, 1962.

Davison, M. J., Average diurnal characteristics of geomagnetic power spectrums in the period range 4.5 to 1000 seconds, J. Geophys. Res., 69, 5116-5119, 1964.

Dessler, A. J., Large amplitude hydromagnetic waves above the ionosphere, J. Geophys. Res., 63, 507-511, 1958.

Duncan, R. A., Some studies of geomagnetic micropulsations, J. Geophys. Res., 66, 2087-2094, 1961.

Dungey, J. W., Electrodynamics of the outer atmosphere, Ionosph. Res. Lab. Sci. Rpt. No. 69, Penn. State Univ., 1954.

Ellis, G. R. A., Geomagnetic micropulsations, Australian J. Phys., 13, 626-632, 1961.

Fejer, J. A., Hydromagnetic wave propagation in the ionosphere, J. Atm. and Terr. Phys., 18, 135-146, 1960.

Forsythe, G. E., and W. R. Wasow, Finite Difference Methods for Partial Differential Equations, John Wiley, New York, 1960.

Francis, W. E., and R. Karplus, Hydromagnetic waves in the ionosphere, J. Geophys. Res., 65, 3593-3600, 1960.

Friedman, H., Ionospheric constitution and solar control, in Research in Geophysics, Vol. I, Hugh Odishaw, ed., Massachusetts Institute of Technology Press, Cambridge, Massachusetts, 1964.

Hildebrand, F. B., Methods of Applied Mathematics, Prentice-Hall, Englewood Cliffs, N. J., 1952.

Holmberg, E. R., A discussion of the origin of rapid periodic fluctuations of the geomagnetic field and a new analysis of observational material, Ph.D. thesis, Univ. of London, 1951.

Jacchia, L. G., Variations in the earth's upper atmosphere as revealed by satellite drag, Smithsonian Astrophys. Obs., 1962.

Jacobs and Sinno, World-wide characteristics of geomagnetic micropulsations, Geophys. Journ. Roy. Astr. Soc., 3, 333-353, 1960.

Jacobs, J. A., Y. Kato, S. Matsushita, V. A. Troitskaya, Classification of geomagnetic micropulsations, J. Geophys. Res., 69, 180-181, 1964.

Jacobs, J. A., and T. Watanabe, Propagation of hydromagnetic waves in the lower exosphere and the origin of short period geomagnetic rapid pulsations, J. Atmos. Terr. Phys., 24, 413-434, 1962.

Johnson, F. S., Satellite Environment Handbook, Stanford Univ. Press, Stanford, California, 1961.

Kato, Y., and T. Saito, Preliminary studies on the daily behavior of rapid pulsation, J. of Geomagnetism and Geoelectricity, 10, 221-225, 1959.

Kato, Y. and T. Watanabe, A survey of observational knowledge of the geomagnetic pulsations, Sci. Rpt. Tohoku Univ., Ser. 5, Geophys., 8, No. 3, 157-184, 1957.

Kato, Y. and T. Watanabe, Geomagnetic storms in relation to geomagnetic pulsations, J. Geophys. Res., 63, 741-750, 1958.

Li, Ti-Shu, C. E. Prince, Jr., and F. X. Bostick, Jr., Hydromagnetic wave propagation and theoretical power spectra, Univ. of Texas, Electrical Eng. Res. Lab. Rpt. No. 134, 1964.

MacDonald, G. J. F., Spectrum of hydromagnetic waves in the exosphere, J. Geophys. Res., 66, 3669-3670, 1961.

Madden, T. R., personal communication, 1964.

Madden, T. R., personal communication, 1965.

Madden, T. R., and W. B. Thompson, Low-frequency electromagnetic oscillations of the earth-ionosphere cavity, Geophysics Lab. Rpt., Massachusetts Institute of Technology, 1964.

Maple, E., Geomagnetic oscillations at middle latitudes, part I, J. Geophys. Res., 64, 1395-1409, 1959.

Martyn, D. F., The normal F region of the ionosphere, Proc. IRE, 47, 147-155, 1959.

Millman, G. H., V. C. Pineo, and D. P. Hynek, Ionospheric investigations by the Faraday rotation of incoherent backscatter, J. Geophys. Res., 69, 4051-4066, 1964.

Ness, N. F., T. L. Skillman, C. S. Scearce, and J. P. Heppner, Magnetic field fluctuations on the earth and in space, J. of the Physical Society of Japan, 17, Sup A-II, 27-33, 1962.

Nicolet, M., Density of the heterosphere related to temperature, Smithsonian Astrophys. Obs., Special Rpt. No. 75, 1961.

Nisbet, J. S., and S. A. Bowhill, Electron densities in the F region of the ionosphere from rocket measurements, J. Geophys. Res., 65, 3609-3614, 1960.

Nishida, A., Ionospheric screening effect and storm sudden commencement, J. Geophys. Res., 69, 1861-1874, 1964.

Orange, A. S., and F. X. Bostick, Jr., Magnetotelluric micropulsations at widely separated stations, J. Geophys. Res., 70, 1407-1413, 1965.

Oshima, H., Pc and geomagnetic disturbances, Memoirs of the Kakioka Magnetic Observatory, 9, No. 2, 1-13, March, 1960.

Prince, C. E., and F. X. Bostick, Jr., Ionospheric transmission of transversely propagated plane waves at micropulsation frequencies and theoretical power spectrums, J. Geophys. Res., 69, 3213-3234, 1964.

Prince, C. E., Jr., F. X. Bostick, and H. W. Smith, A study of the transmission of plane hydromagnetic waves through the upper atmosphere, Univ. of Texas, Electrical Eng. Res. Lab. Rpt. No. 134, 1964.

Ratcliffe, J. A., ed., Physics of the Upper Atmosphere, Academic Press, New York, 1960.

Sagalyn, R. C., M. Smiddy, and J. Wisnia, Measurement and interpretation of ion density distributions in the daytime F region, J. Geophys. Res., 68, 199-211, 1963.

Saito, T., Period analysis of geomagnetic pulsations by a sona-graph method, Sci. Rpt., Tohoku Univ., Ser. 5, Geophys. 12, 106-113, 1960.

Saito, T., Mechanisms of geomagnetic continuous pulsations and physical states of the exosphere, J. of Geomagnetism and Geoelectricity, 16, 115-151, 1964.

Santirocco, R. A., and D. G. Parker, The polarization and power spectrums of Pc micropulsations in Bermuda, J. Geophys. Res., 68, 5545-5558, 1963.

Smith, H. W., L. D. Provazek, and F. X. Bostick, Jr., Directional properties and phase relations of the magnetotelluric fields at Austin, Texas, J. Geophys. Res., 66, 879-888, 1961.

Thompson, W. B., A layered model approach to the earth-ionosphere cavity resonance problem, Ph.D. thesis, Massachusetts Institute of Technology, 1963.

Troitskaya, V. A., Rapid variations of the electromagnetic field of the earth, in Research in Geophysics, Vol. I, Hugh Odishaw, ed., Massachusetts Institute of Technology Press, Cambridge, Massachusetts, 1964.

Yanagihara, K., Geomagnetic pulsations in middle latitudes, Memoirs of the Kakioka Magnetic Observatory, 9, No. 2, 15-74, 1960.

Young, D. M., Numerical solution of elliptic and parabolic partial differential equations, in Survey of Numerical Analysis, J. Todd, ed., McGraw-Hill, New York, 1962.

Westphal, K. O., Oscillations of the earth's outer atmosphere and micropulsations, Ph.D thesis, Univ. of British Columbia, 1961.

BIOGRAPHICAL NOTE

R. J. Greenfield attended high school in Hollywood, Florida. In 1958 he received a B.S. in Geology and Geophysics from M.I.T. He spent one year of study at the California Institute of Technology and one semester at U.C.L.A.

Mr. Greenfield was employed for two years by the International Business Machines Corp.

In 1962 he returned to the M.I.T. graduate school and received his M.S. degree. His masters thesis was done under the direction of Professor S. M. Simpson.